

Supplementary Materials for

Production of H₂ at Fast Rates Using a Nickel Electrocatalyst

in Water/Acetonitrile Solutions

*Wesley A. Hoffert, John A. S. Roberts, R. Morris Bullock and Monte L. Helm**

correspondence to: monte.helm@pnnl.gov

This PDF file includes:

Table of Contents
Materials and Methods
Supplementary Text
Figs. S1 to S32
Tables S1 to S7
References (1-6)

Table of Contents

Materials and Methods	4
Materials	4
Instrumentation	4
Catalytic Hydrogen Production. <i>Overpotential, referencing, i_p, and i_{cat} determination, and conditions for controlled potential electrolysis.</i>	5
X-ray Diffractometry	5
Syntheses.....	6
Supplementary Text	7
X-ray Structure of Complex 1	7
Example Calculation of TOF	8
Fig. S1 CVs for sample TOF calculation.....	8
Table S1 Electrochemical data for TOF calculation	9
Table S2 Sample TOF calculation	9
Fig. S2 Plot of TOF vs overpotential.....	10
Fig. S3 Plots of OCP vs[HClO ₄] and E_{cat} vs [HClO ₄]	11
Fig. S4 Scatter plot of log TOF vs overpotential for nickel bis(diphosphine) proton reduction catalysts.....	12
Fig. S5 Plot of i_{cat} vs scan rate and corresponding CVs	13
Fig. S6 Plot of i_{cat} vs catalyst concentration	14
Fig. S7 Cyclic voltammogram of 3.58 M HClO ₄ background and catalytic wave	15
Fig S8 CVs of 1 at different scan rates.....	16
Table S3 Tabulated cyclic voltammetry data.....	16
Fig. S9 Plots of i_{cat}/i_p and TOF vs [HClO ₄]	17
Fig S10 Plot of current density vs[HClO ₄].....	18
Fig. S11 CVs of 1 in dry MeCN with various concentrations of [HDMF ⁺] and corresponding TOF vs [HDMF ⁺] plot.....	19
Fig S12 CVs of 1 in MeCN with 1 M H ₂ O and various concentrations of [HDMF ⁺] and corresponding TOF vs [HDMF ⁺] plot.....	20
Fig. S13 CVs of 1 in water/acetonitrile with various concentrations of H ₂ SO ₄ and corresponding TOF vs. [H ₂ SO ₄] plot.....	21
Fig. S14 CVs of 1 in water/acetonitrile with various concentrations of HNTf ₂ and corresponding TOF vs. [HNTf ₂] plot.....	22

Table S4 Tabulated Voltammerty data for 1 showing i_{cat} in various %water solvent compositions	23
Fig. S15 Plot of OCP vs. $[H_2SO_4]$	24
Fig. S16 OCP vs. time for various concentrations of H_2SO_4 and $HClO_4$	25
Fig. S17 CVs of 1 at high $HClO_4$ concentrations and after addition of NaOH	26
Fig. S18 Absorbance at λ_{max} for 1 at high $HClO_4$ concentrations and after addition of NaOH	26
Fig S19 CVs of 1 in H_2O , 33% CH_3CN by volume at various scan rates.....	27
Fig. S20 CV comparison of $[Ni(P^{Ph}_2N^{Ph}_2)_2]^{2+}$ and 1 in H_2O , 33% CH_3CN by volume ...	28
Fig. S21 Correlations between $-\log[acid]$ and pH for H_2SO_4 and $HClO_4$	29
Fig. S22 Plots of i_{cat} vs. pH and log TOF vs pH for 1	30
Fig S23 Determination of $E_{1/2}$ of hydroxymethylferrocene vs. $Fc^{+/0}$	31
Fig S24 CVs of hydroxymethylferrocene and $[Cp_2Co](PF_6)$ under neutral and acidic conditions.....	32
Fig. S25 Gas chromatography data from a controlled potential electrolysis experiment with 1	33
Table S5 Tabulated gas chromatography data from a controlled potential electrolysis experiment with 1	33
Fig. S26 Plot of turnover number (TON) and charge passed vs time for an extended CPE experiment with 1	34
Fig. S27 Plot of the normalized absorbance at 480 nm over time with various $HClO_4$ concentrations and UV-Vis spectra for 1	35
Fig. S28 Determination of the half-life for 1 with different concentrations of $HClO_4$	36
Fig. S29 $^{31}P\{^1H\}$ NMR spectrum of $P^{Ph}_2N^{C_6H_4OH}_2$ ligand in THF	37
Fig. S30 1H NMR spectrum of $P^{Ph}_2N^{C_6H_4OH}_2$ ligand in d_8 -THF	38
Fig. S31 $^{31}P\{^1H\}$ NMR spectrum of complex 1 in CH_3CN	39
Fig. S32 1H NMR spectrum of complex 1 in CD_3CN	40
Table S6 Crystallographic data for complex 1	41
Table S7 Selected bond distances and angles for 1	42
References	43

Materials and Methods

Materials

All manipulations were carried out using standard Schlenk or inert-atmosphere glovebox techniques using oven-dried glassware, unless otherwise indicated. Non-aqueous solvents were purified by sparging with N₂ and passage through neutral alumina, using a solvent purification system (PureSolv™, Innovative Technologies, Inc.). Water was dispensed from a Millipore MilliQ purifier ($\rho = 18.2 \text{ M}\Omega\cdot\text{cm}$) and was degassed using three freeze-pump-thaw cycles prior to use. [Ni(CH₃CN)₆](BF₄)₂ (1) and PhP(CH₂OH)₂ (2) were prepared using literature methods. All other chemicals were purchased commercially and were used as received.

Instrumentation

¹H and ³¹P spectra were recorded on Varian spectrometers (500 MHz or 300 MHz) at 23 °C. All ¹H chemical shifts have been internally calibrated to the monoprotio impurity of the deuterated solvent, and all ¹H chemical shifts are referenced to tetramethylsilane. The ³¹P NMR spectra were referenced to external phosphoric acid. Elemental analyses were carried out by Atlantic Microlab, Norcross, GA 30071. pH measurements were obtained with a Thermo Orion Dual Star meter equipped with a micro pH electrode. To account for solvent effects, pH readings made after calibration with aqueous buffers (^spH) in H₂O/CH₃CN mixtures were adjusted to ^spH values by the method of Bosch and coworkers (3). UV-Vis data was collected under dinitrogen with an Ocean Optics USB2000+ spectrometer. All electrochemical experiments were carried out under an atmosphere of nitrogen using hydroxymethylferrocene ($E_{1/2} = -0.073 \text{ V vs. Fc}^{+/0}$ in acetonitrile, see Figure S23) as an internal reference. For all cyclic voltammograms, the assumption is made that the $E_{1/2}$ for hydroxymethylferrocene is invariant with solvent composition and acid concentration; all potentials are reported versus the ferrocenium/ferrocene couple. To prepare solutions for electrochemical experiments, **1** was first dissolved in dry acetonitrile followed by addition of an appropriate amount of aqueous electrolyte. Cyclic voltammograms were acquired using a CH Instruments 620D or 660C potentiostat equipped with a standard three-electrode cell. Prior to the acquisition of each cyclic voltammogram, the working electrode (1 mm PEEK-encased glassy carbon, surface area = 0.0068 cm²) was polished using diamond paste followed by rinsing with water. The reference was an Ag/AgCl electrode equipped with a Teflon tip and the counter electrode was a 3 mm glassy carbon rod. Controlled potential electrolysis was performed in a sealed cell (volume = 355 mL) using a Vycor-separated Ni-chrome coil counter electrode, Vycor-separated Ag wire reference electrode, and reticulated vitreous carbon working electrode. A cyclic voltammogram was recorded immediately prior to electrolysis to determine the reducing potential. A BASi Epsilon potentiostat combined with an auxiliary BASi PWR-3 power module was used to supply the reducing current. Gas analysis for H₂ was performed using an Agilent 6850 gas chromatograph with a thermal conductivity detector fitted with a 10 ft Supelco 1/8" Carbosieve 100/120 column, calibrated with two H₂/N₂ gas mixtures of known composition.

Catalytic Hydrogen Production. Overpotential, referencing, i_p , and i_{cat} determination, and conditions for controlled potential electrolysis.

All catalytic experiments were carried out at ambient temperature (25 °C). Solutions of electrolyte (0.2 M in water) and catalyst were prepared in the glovebox. The mineral acid solutions (HClO₄ and H₂SO₄) were prepared outside of the glovebox, titrated with standardized NaOH solution to accurately determine the concentration, then degassed with three freeze-pump-thaw cycles prior to using. A solution of aqueous HNTf₂ of known concentration was prepared inside the glovebox using volumetric dilution with degassed water. The procedure for determining the thermodynamic potential for proton reduction was adapted from the open circuit potential (OCP) method that has previously been described (33). Overpotentials were taken as the difference between $E_{1/2}^{cat}$ and the thermodynamic potential E_{H^+/H_2} (OCP at Pt electrode) for the reduction of acid to free base plus one half equivalent H₂ gas, with both potentials referenced directly to hydroxymethylferrocenium/hydroxymethylferrocene. The potentials were then referenced to ferrocenium/ferrocene by subtracting 0.073 V ($E_{1/2}$ of [Cp(C₅H₄CH₂OH)Fe] = -0.073 V vs. Fc⁺⁰). The i_p values were conservatively chosen by measuring the largest difference between the peak and baseline currents in the absence of acid. The potentials at which i_{cat} values were measured were located by finding the most positive potential for each catalytic wave beyond the $E_{1/2}^{cat}$ for which the derivative of the $i - E$ trace is approximately zero. Although $E_{1/2}^{cat}$ stays constant, these potentials shift to more negative values as the acid concentration is increased and were approximately 130-330 mV negative of $E_{1/2}^{cat}$. To determine Faradic efficiency, a controlled potential electrolysis was performed with a 0.3 mM solution of the catalyst in the presence of 0.99 M HClO₄ and trace hydroxymethylferrocene as an internal reference. The electrolysis was performed at -1.23 V vs Fc⁺⁰. The solution contained 43% acetonitrile by volume.

X-ray Diffractometry

Crystals of **1** were grown by diethyl ether vapor diffusion into a concentrated solution of **1** in acetonitrile. Single crystals were coated in Paratone to facilitate manipulation. The crystals were supported on a Cryoloop and mounted on a Bruker Kappa Apex 2 CCD diffractometer under a stream of cold dinitrogen. All data collection was performed using Mo K α radiation and a graphite monochromator. Initial lattice parameters were determined from reflections with $I > 20\sigma$ harvested from 36 frames; these parameters were later refined against all data. Data collection strategies were targeted for a minimum of 0.85 Å resolution with fourfold redundancy. Frames were collected with 30 second exposures, but few reflections beyond ca. 0.95 Å resolution were found. Data were integrated and corrected for absorption effects with the Apex II software package. The structure was initially solved by direct methods and refined with the SHELXTL software package, and, all non-hydrogen atoms with the exception of partial-occupancy carbons were refined anisotropically. Friedel pairs were merged prior to refinement. Initially, the structure was solved in the monoclinic C2 space group, ADDSYM was later used to add the additional orthorhombic symmetry. The final solution was obtained in the C222 space group. Hydrogen atoms were added at the ideal positions and were refined using a riding model in which the displacement parameters were set at 1.2 times that of the attached carbon atom (1.5 times for methyl carbons).

Both of tetrafluoroborate anions and the nickel complex reside on a crystallographic two-fold rotation axes. For the complex, the two-fold axis is co-linear with the CH₃CN ligand. One of the tetrafluoroborates is rotationally disordered; this was modeled by setting the occupancy of each of the disordered components to 50%. Platon SQUEEZE was used to remove the contribution of heavily disordered electron density corresponding to exogenous diethyl ether solvent. The solvent molecules are unrelated to the nickel complex and tetrafluoroborate anions and could not be modeled successfully in the difference map. The SQUEEZE program found 276 electrons in 1754 Å³ of accessible unit cell void volume (4). Since $Z = 4$, this translates to 69 e⁻ per whole complex molecule, consistent with approximately 1.6 exogenous diethyl ether molecules (42 e⁻ each), which nearly matches the obtained elemental analysis of a crystalline sample.

Syntheses

1,5-bis(*p*-hydroxyphenyl)-3,7-bis(phenyl)-1,5-diaza-3,7-diphosphacyclooctane (P^{Ph}₂N^{C₆H₄OH}₂). A 100 mL Schlenk flask was charged with solid bis(hydroxymethyl)phenylphosphine (0.500 g, 2.94 mmol), 4-aminophenol (0.321 g, 2.94 mmol) and 20 mL of degassed absolute ethanol. The resulting clear, colorless solution was heated for 2 h at 60 °C, during which time a white solid precipitated. The reaction mixture was cooled to room temperature, and the white solid product was collected by filtration, washed with ethanol (3 × 3 mL) and tetrahydrofuran (3 × 1 mL) and dried in vacuo to afford the final product (550 mg, 1.13 mmol, 77%). ³¹P{¹H} NMR (*d*₈-THF): δ -50.4 ppm. ¹H NMR (*d*₈-THF): δ 7.59 (t, $J = 6$ Hz, 4H, *o*-C₆H₅); 7.41 (m, 4H, *m*-C₆H₅); 7.36 (m, 2H, *o*-C₆H₅); 7.31 (s, 2H, C₆H₄OH); 6.57 (m, 8H, C₆H₄OH); 4.29 (m, 4H, PCH₂N); 4.14 (m, 4H, PCH₂N) ppm. Analysis calculated for C₂₈H₂₈N₂P₂O₂: C, 69.13%; H, 5.80%; N, 5.76%. Found: C, 68.85%; H, 5.96%; N, 5.73%.

[Ni(P^{Ph}₂N^{C₆H₄OH}₂)₂(CH₃CN)](BF₄)₂ (**1**). A blue solution of [Ni(CH₃CN)₆](BF₄)₂ (91 mg, 0.19 mmol) in acetonitrile (3 mL) was added to a stirred slurry of P^{Ph}₂N^{C₆H₄OH}₂ (186 mg, 0.38 mmol) in acetonitrile (3 mL), causing the mixture to turn deep red. After stirring for 5 minutes, the mixture was filtered through a plug of Celite, and the volume to the solution was reduced to ca. 1 mL by evaporation. Addition of excess diethyl ether (15 mL) caused an orange solid to precipitate. The solid was collected by filtration, washed with diethyl ether (3 × 2 mL), and dried under vacuum to afford the final product (209 mg, 0.17 mmol, 91%). Single crystals suitable for X-ray analysis were grown by diffusion of diethyl ether vapor into a concentrated solution of the product in acetonitrile. ³¹P{¹H} NMR (CD₃CN): δ 6.1 ppm. ¹H NMR (CD₃CN): δ 7.35 (t, $J = 8$ Hz, 4H, *p*-C₆H₅); 7.31 (m, 8H, *m*-C₆H₅); 7.18 (m, 8H, C₆H₄OH); 7.12 (t, $J = 8$ Hz, 8H, *o*-C₆H₅); 6.88 (s, 4H, C₆H₄OH); 6.85 (m, 8H, C₆H₄OH); 4.11 (d, $J = 14$ Hz, 8H, PCH₂N); 3.78 (d, $J = 13$ Hz, 8H, PCH₂N) ppm. Analysis calculated for C₆₂H₆₉B₂F₈N₅NiO₅P₄ (**1** · Et₂O): C, 56.40%; H, 5.27%; N, 5.30%. Found: C, 56.40%; H, 5.46%; N, 5.46%.

Supplementary Text

X-ray Structure of Complex 1

The structure of **1** consists of the nickel(II) complex with a bound acetonitrile ligand, two non-coordinated tetrafluoroborate anions, and approximately 1.5 disordered diethyl ether molecules which could not be modeled satisfactorily. The structure of the complex cation resembles that of previously characterized $[\text{Ni}(\text{P}^{\text{Ph}}_2\text{N}^{\text{R}'}_2)_2]^{2+}$ complexes where R is a *para*-substituted phenyl group, and all of the Ni–P bond distances and ligand bite angles are typical for Ni^{II} complexes with two 8- $\text{P}^{\text{Ph}}_2\text{N}^{\text{R}'}_2$ ligands. The core geometry is best described as a distorted trigonal bipyramid, with the distortion due in part to steric interactions between the adjacent phenyl substituents. There is also an offset π - π stacking interaction ($d_{\text{ph-ph}} = \text{ca. } 3.4 \text{ \AA}$) between the phenyl rings attached to adjacent phosphine ligands. The dihedral angle between the P–Ni–P planes is 39.11° , which is slightly smaller than for related $[\text{Ni}(\text{P}^{\text{Ph}}_2\text{N}^{\text{Ph}}_2)_2(\text{CH}_3\text{CN})]^{2+}$ whose dihedral angle was measured to be 44.16° (5).

Example Calculation of TOF

The following represents an example calculation of TOF for **1**. Figure S1 shows the CV's used for the calculations and Tables S1 and S2 summarize the experimental data and calculation procedure.

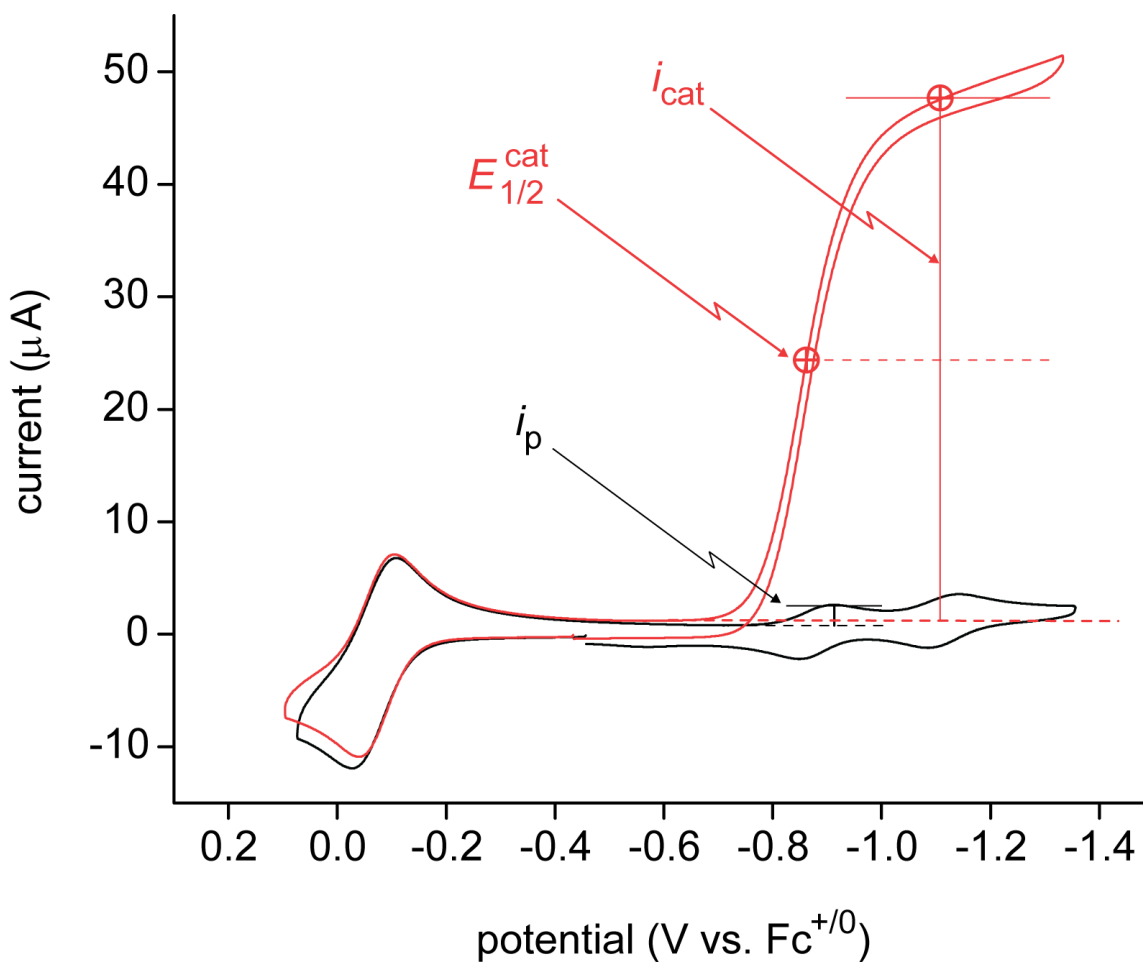


Fig. S1

Cyclic voltammograms of 0.32 mM **1**, [Ni(P^{Ph}₂N^{4-C6H4OH})₂]²⁺ (black) overlaid with 0.30 mM **1**, [Ni(P^{Ph}₂N^{4-C6H4OH})₂]²⁺ (red) with 0.19 M HClO₄. Conditions: 1 mm glassy-carbon working electrode; scan rate 1 V s⁻¹.

Table S1

Raw experimental data from cyclic voltammograms in Figure S1.

Initial [1]	Volume 1	Initial [HClO ₄]	Volume HClO ₄	<i>i</i> _p (μA)	<i>i</i> _{cat} (μA)
0.32 M	1.0 mL	4.0 M	0.050 mL	1.82	46.6

Table S2

Calculation of TOF for the cyclic voltammograms in Figure S1.

Operation	Equation	Calculation
Dilution corrected <i>i</i> _p value	$i_p \times \frac{\text{initial volume}}{\text{final volume}}$	$(1.82 \times 10^{-6}) \times \frac{1.00}{1.05} = 1.73 \times 10^{-6}$
Calculation of the ratio of catalytic current to non-catalytic current	$\frac{i_c}{i_p}$	$\frac{4.66 \times 10^{-5}}{1.73 \times 10^{-6}} = 26.9$
Using the $\frac{i_c}{i_p}$ ratio to calculate TOF	$\text{TOF} = 1.94 \cdot v \left(\frac{i_{\text{cat}}}{i_p} \right)^2$	$\text{TOF} = 1.94 \text{ V}^{-1} \times 1.0 \text{ V s}^{-1} \times (26.9)^2 = 1400 \text{ s}^{-1}$

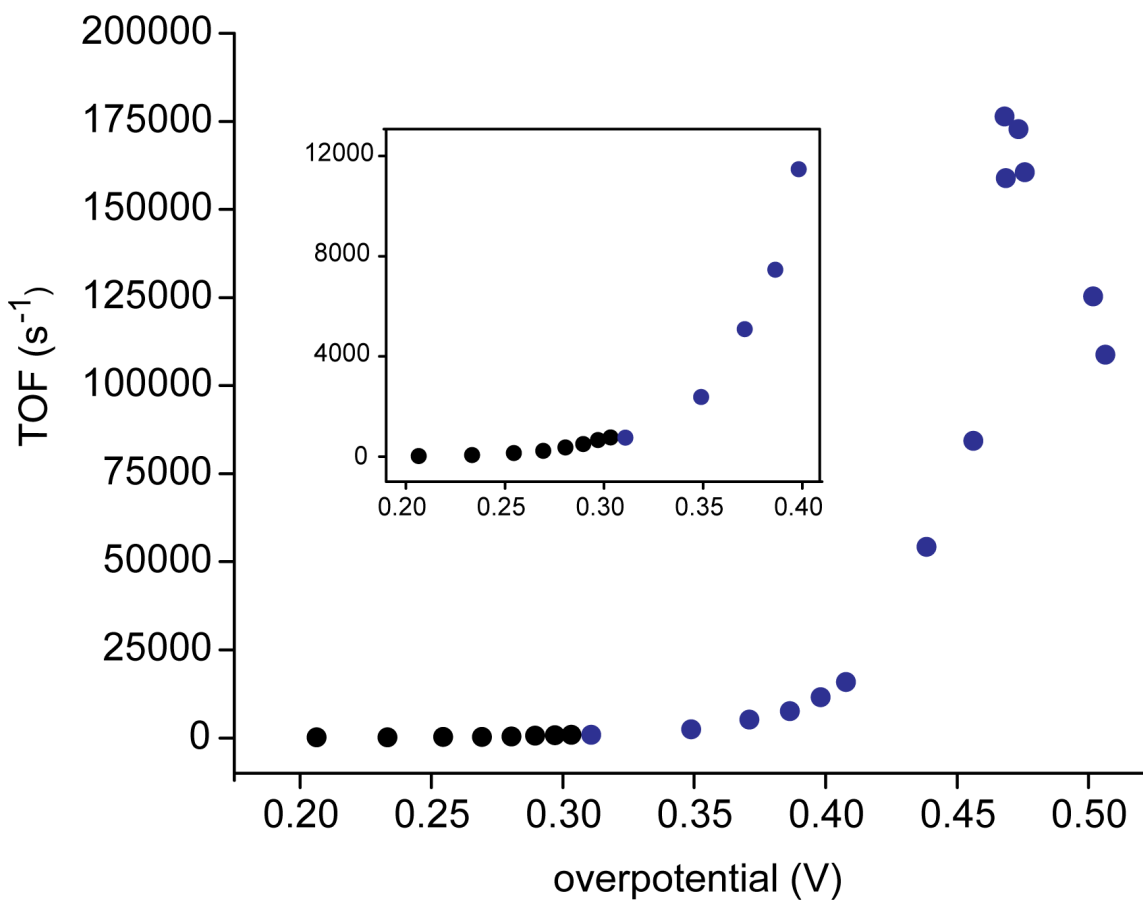


Fig. S2

Plot of the turnover frequency (TOF) vs. overpotential for **1** using H₂SO₄ (black data points) and HClO₄ (blue data points). Inset: close-up of the data between 0.20 and 0.40 V.

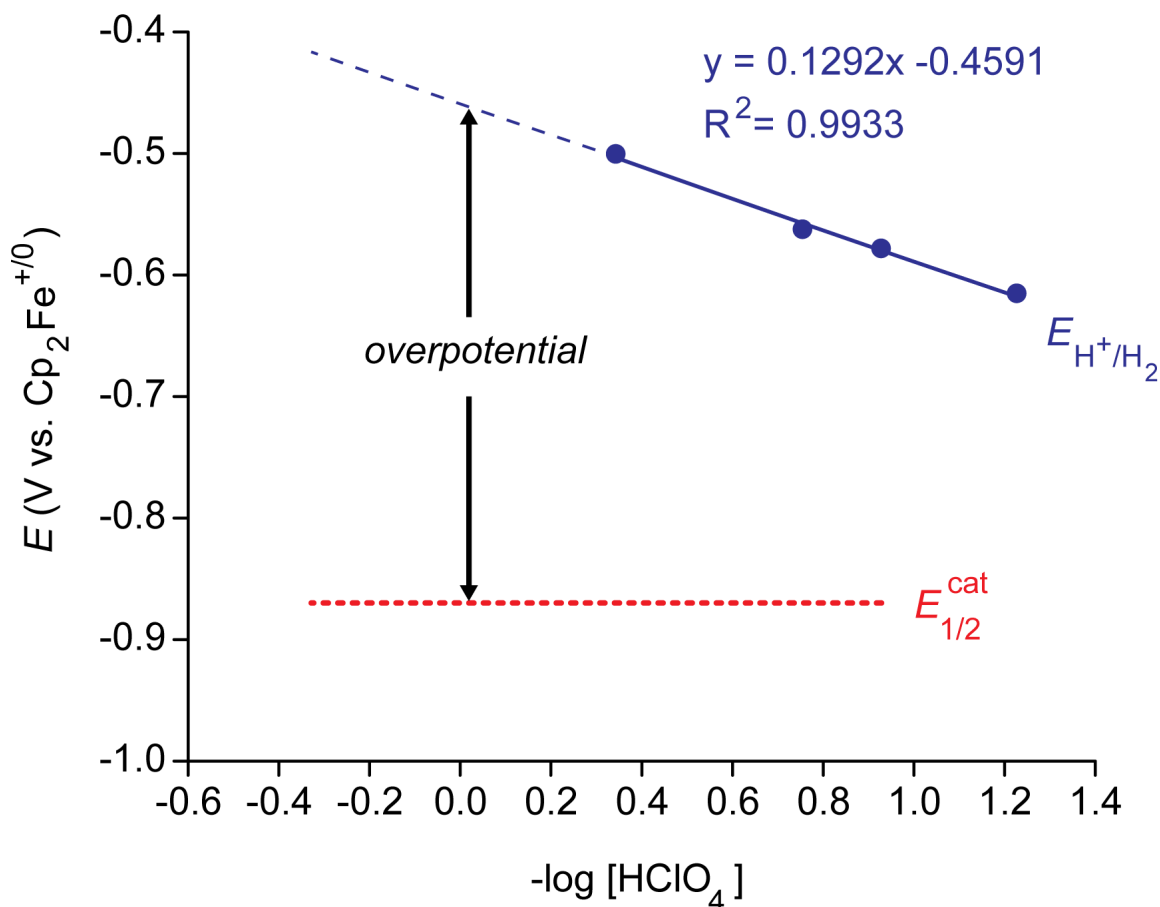


Fig. S3

Plot of the open circuit potential vs. $[\text{Cp}_2\text{Fe}]^{+/0}$ at a Pt electrode ($E_{\text{H}^+/\text{H}_2}$) vs. $-\log$ of $[\text{HClO}_4]$ measured in molarity (blue data points and blue line) and the measured half-wave potential for the catalytic wave of **1** (-0.87 V vs. $[\text{Cp}_2\text{Fe}]^{+/0}$ at all acid concentrations, red dashed line). As indicated, the difference between the two potentials at a given acid concentration corresponds to the overpotential for proton reduction. See Materials and Methods and Figure S16 for details concerning the collection of the open circuit potential data (33).

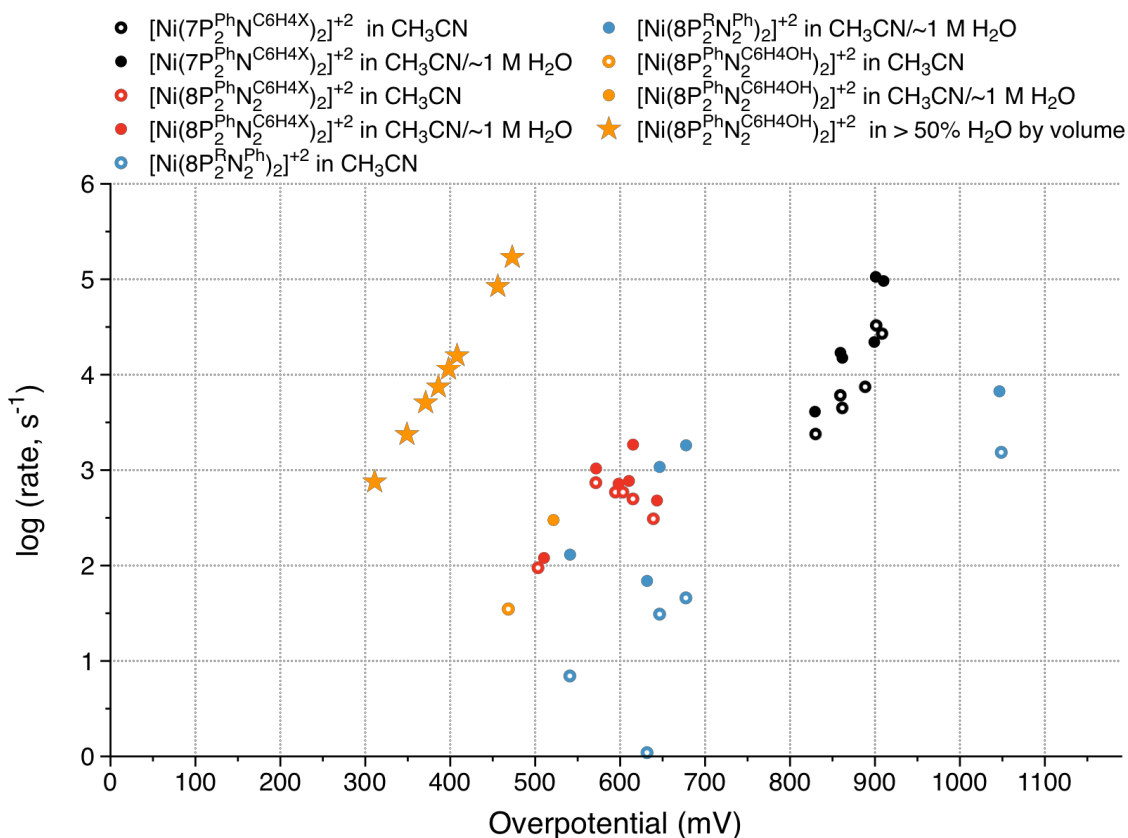


Fig. S4

Scatter plot of the log of maximum TOF (measured in s^{-1}) vs. overpotential for several previously published Ni(II) bis-diphosphine H_2 production catalysts from our laboratory (filled and open circles) and **1** at various TOF. For the sake of comparison, the overpotentials for all catalysts were determined from the difference between $E_{1/2}^{\text{cat}}$ and the thermodynamic potential for proton reduction with a given concentration of $[\text{HDMF}^+](\text{OTf})$ in acetonitrile except for the starred points, which correspond to **1** with various concentrations of HClO_4 in predominantly aqueous conditions as discussed in the main text. The thermodynamic potential for proton reduction with HDMF^+ in CH_3CN has been reported as: $E_{\text{H}^+/\text{H}_2}$ (V vs. $\text{Fc}^{+/0}$) = $0.0720 \times \log([\text{HDMF}^+]) - 0.192$. (4) Open circles correspond to anhydrous CH_3CN conditions, closed circles correspond to data recorded in CH_3CN with ca. 1M H_2O present. Black = $[\text{Ni}(\text{7P}_2^{\text{Ph}}\text{N}_2^{\text{R}})_2]^{2+}$ complexes, blue = $[\text{Ni}(\text{8P}_2^{\text{R}}\text{N}_2^{\text{Ph}})_2]^{2+}$ complexes, red = $[\text{Ni}(\text{8P}_2^{\text{Ph}}\text{N}_2^{\text{R}})_2]^{2+}$ complexes, orange = **1**.

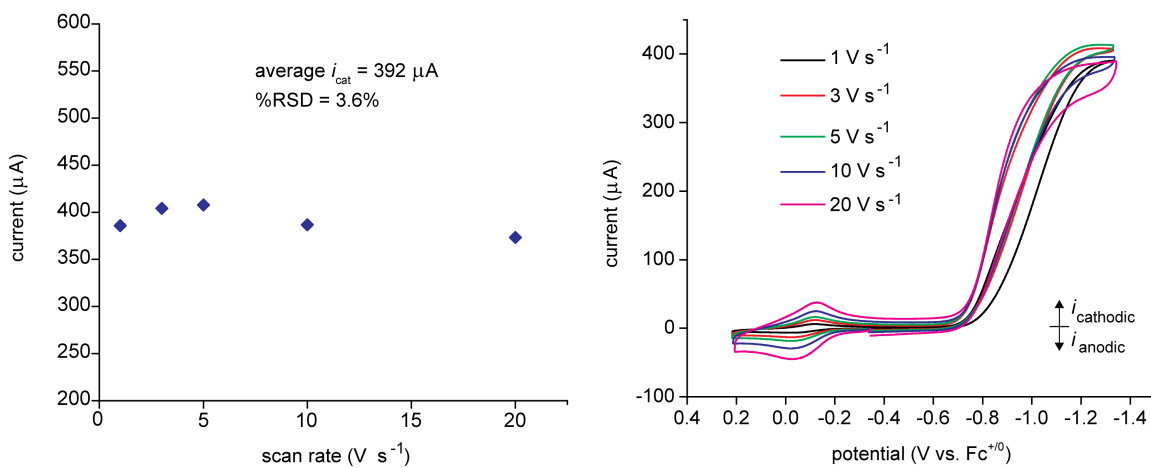


Fig. S5

Left: plot of i_{cat} vs. scan rate for a solution containing 0.21 mM **1** and 1.99 M $HClO_4$ (left) and the corresponding cyclic voltammograms (right). Since i_{cat} is independent of scan rate, the catalytic process is not diffusion-controlled, making the Saveant-Vianello treatment (calculation described in Table S2) valid (6). The data were recorded in H_2O , 38% CH_3CN by volume (0.1 M $NaClO_4$).

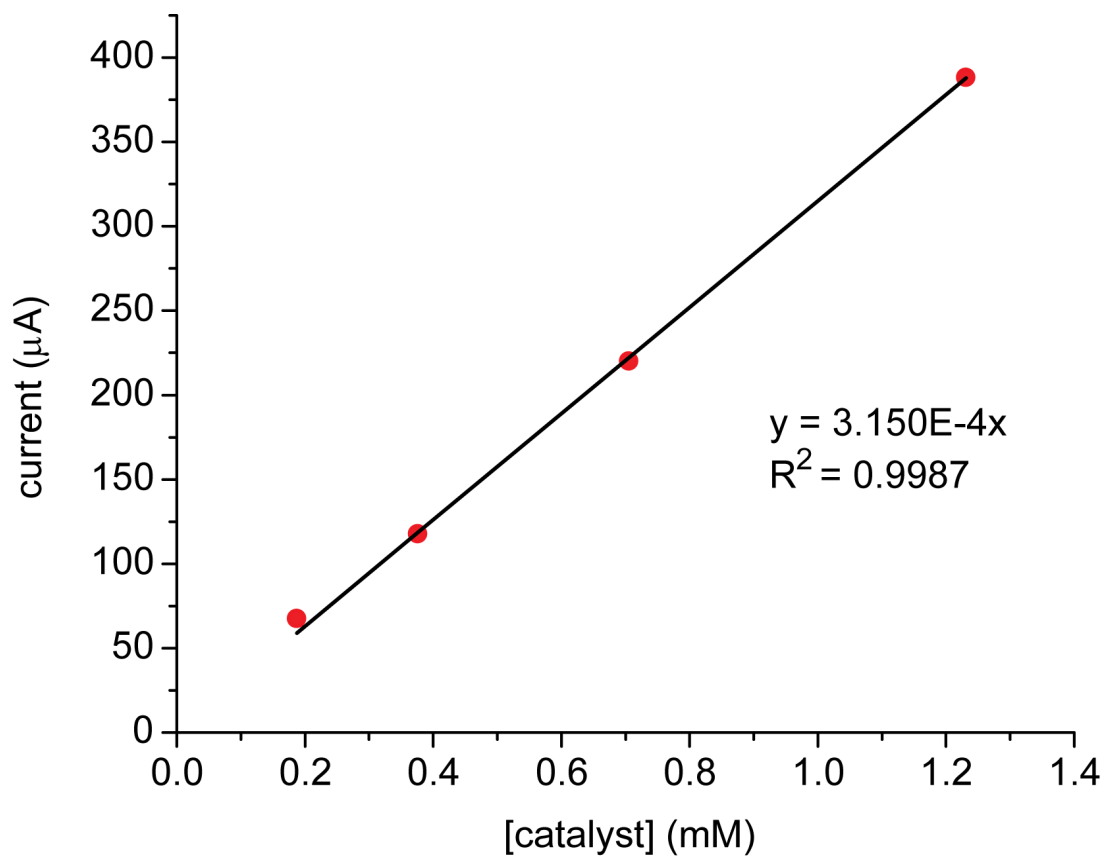


Fig. S6

Plot of i_{cat} vs. catalyst concentration. The first-order dependence of i_{cat} on catalyst concentration makes the Saveant-Vianello treatment (calculation described in Table S2) valid (41). For all data, the concentration of HClO_4 was 0.53 M.

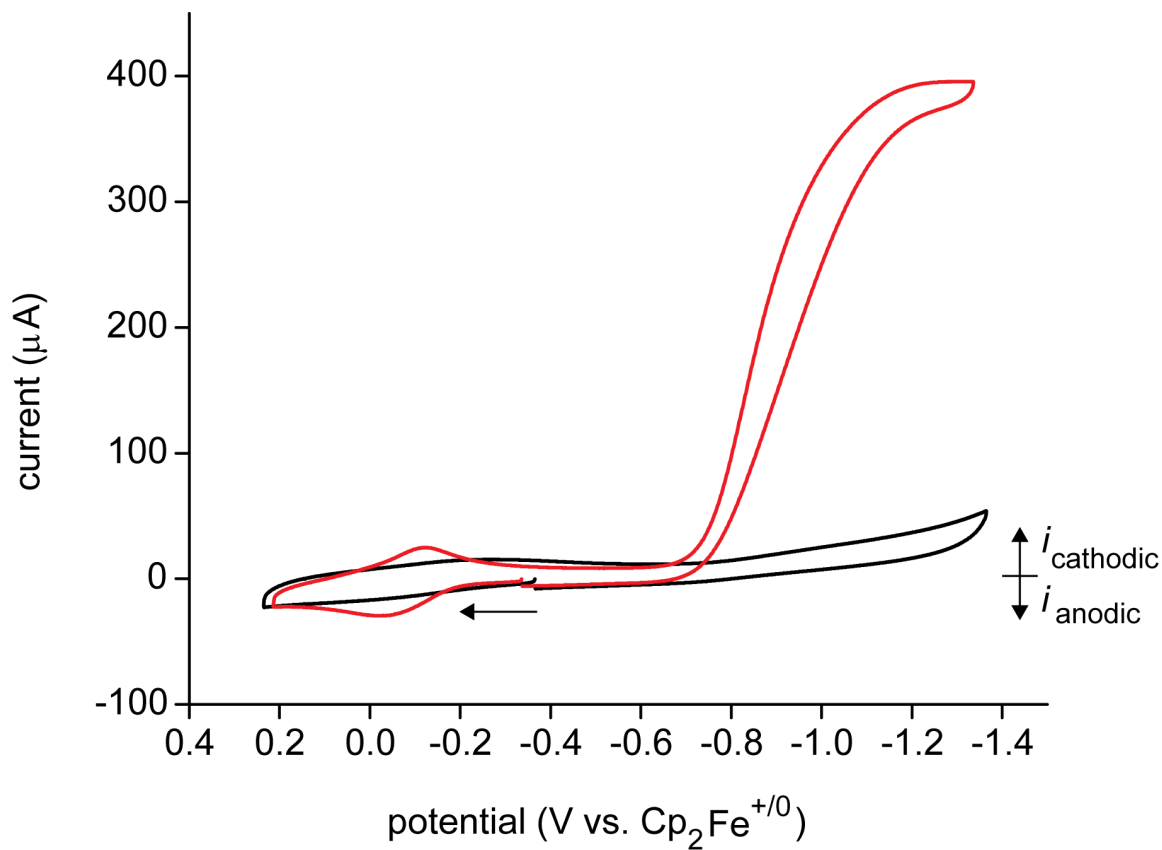


Fig. S7

Cyclic voltammograms of 3.58 M HClO₄ in H₂O, 30% acetonitrile by volume (black trace) and a solution containing 0.21 mM **1**, hydroxymethylferrocene, and 1.99M HClO₄ in H₂O, 38% acetonitrile by volume (0.1 M NaClO₄) (red trace). Scan rate = 10 V s⁻¹.

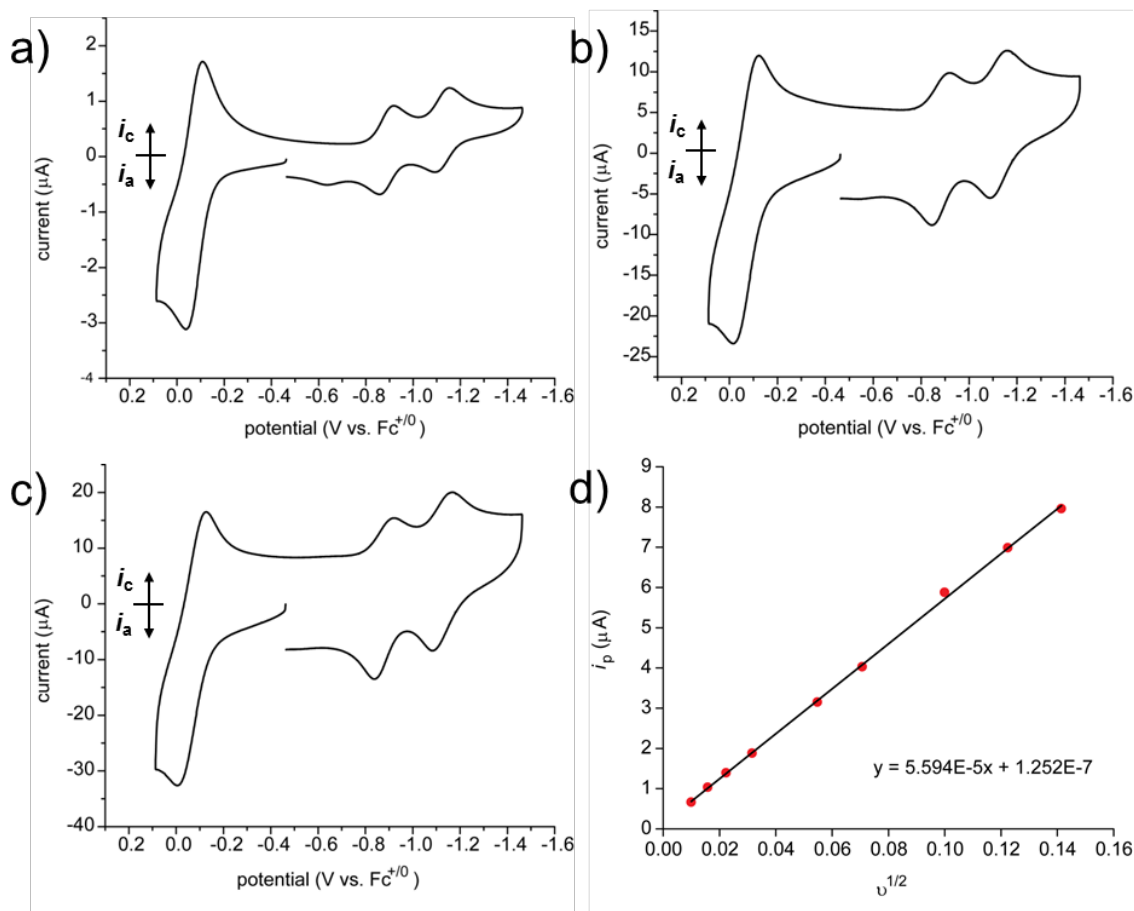


Fig S8.

Cyclic voltammograms of a 0.36 mM solution of **1** and hydroxymethylferrocene in 1:1 H₂O/CH₃CN by volume (0.1 M NaClO₄) at scan rates of a) 0.1 V s⁻¹; b) 5 V s⁻¹; and c) 10 V s⁻¹. d) Plot of cathodic peak current *i*_p for the Ni(II/I) couple versus the square root of scan rate *v*^{1/2} measured in V s⁻¹.

Table S3.

Cyclic voltammetry *E*_{1/2} and Δ*E*_p data (V) for hydroxymethylferrocene and **1** in 1:1 H₂O/CH₃CN by volume (0.1 M NaClO₄).

	<i>E</i> vs. Fc ⁺⁰ (V)	scan rate = 0.1 V s ⁻¹	scan rate = 10 V s ⁻¹
[Cp(C ₅ H ₄ CH ₂ OH)Fe] ⁺⁰	-0.073	Δ <i>E</i> _p = 0.072	Δ <i>E</i> _p = 0.126
1 (Ni II/I)	-0.89	Δ <i>E</i> _p = 0.060	Δ <i>E</i> _p = 0.090
1 (Ni I/0)	-1.14	Δ <i>E</i> _p = 0.069	Δ <i>E</i> _p = 0.084

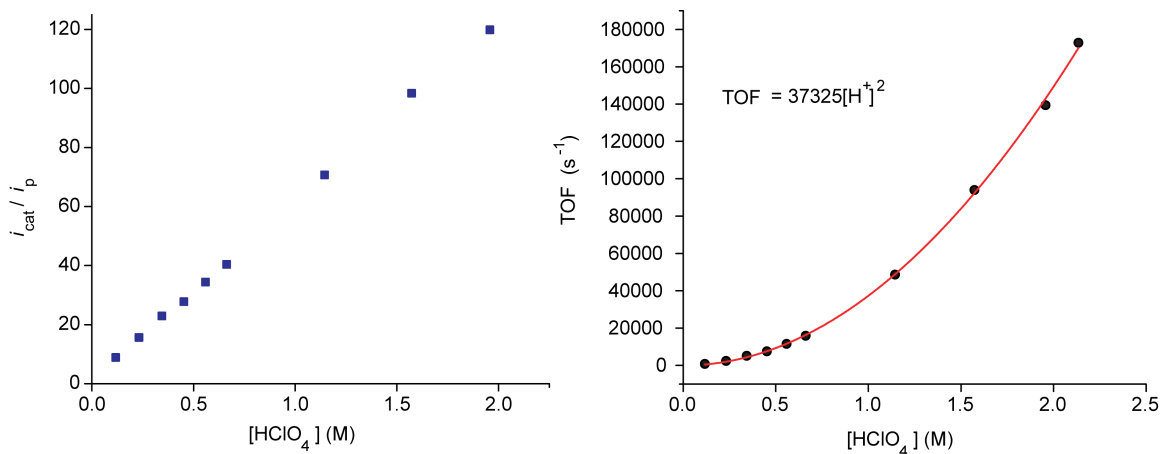


Fig. S9

Left: plot of i_{cat}/i_p vs. acid concentration from 0.1 to 2M $HClO_4$ from data obtained with a $5 V s^{-1}$ scan rate. Since i_{cat}/i_p varies with the square root of TOF, the relationship is linear for a second order process. Right: plot of TOF vs acid concentration from 0.1 to 2 M $HClO_4$, also demonstrating that the reaction is second order in acid. A simple curve fit was used to obtain an empirical rate constant of $37325 M^{-2}\cdot s^{-1}$.

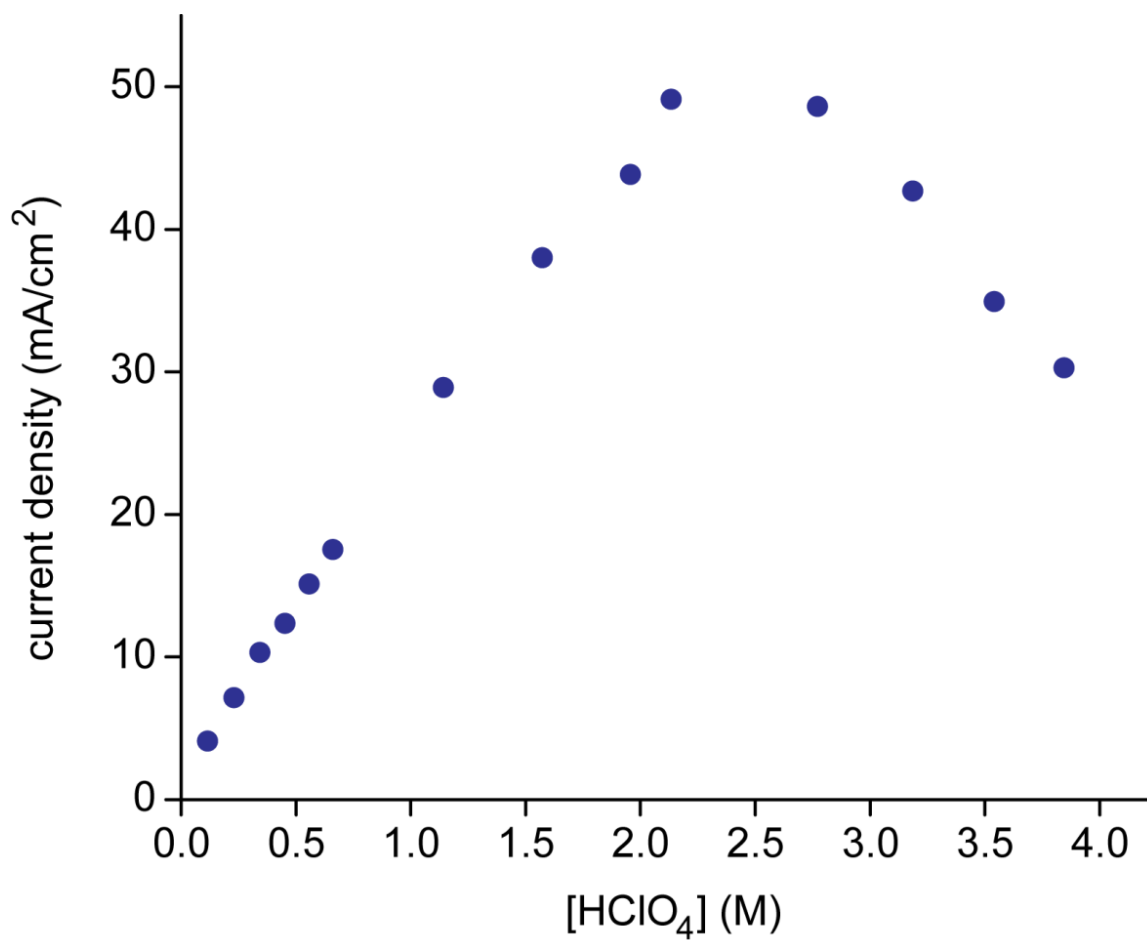


Fig S10

Plot of the current density vs. perchloric acid concentration for **1**. The surface area of the glassy carbon working electrode used was 0.0086 cm².

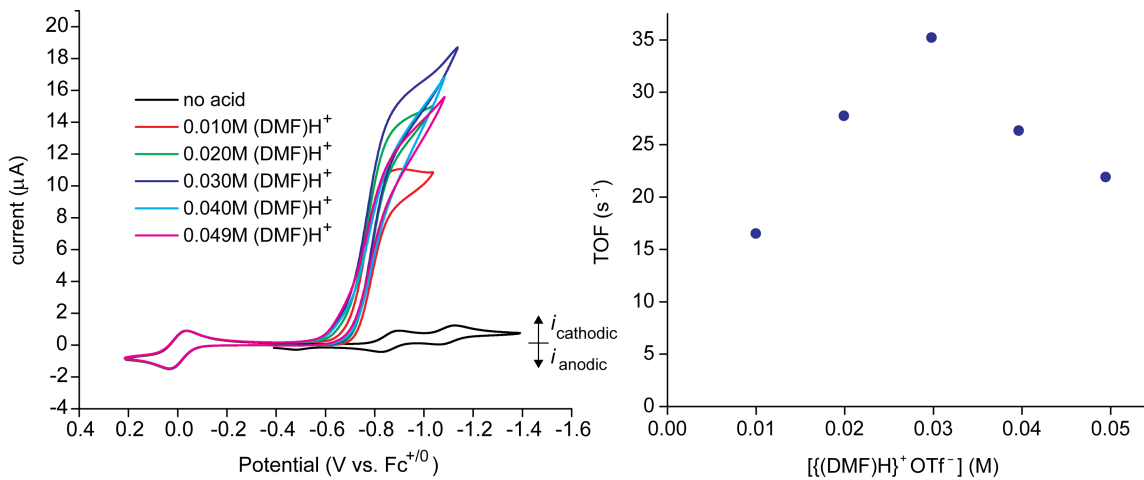


Fig. S11

Left: cyclic voltammograms of **1** in dry CH₃CN (0.1 M ⁿBu₄N⁺PF₆⁻) in the presence of varying concentrations of [(DMF)H]⁺OTf⁻ using ferrocene as the internal reference. Scan rate = 0.05 V s⁻¹. Right: plot of the turnover frequency vs. [(DMF)H]⁺OTf⁻.

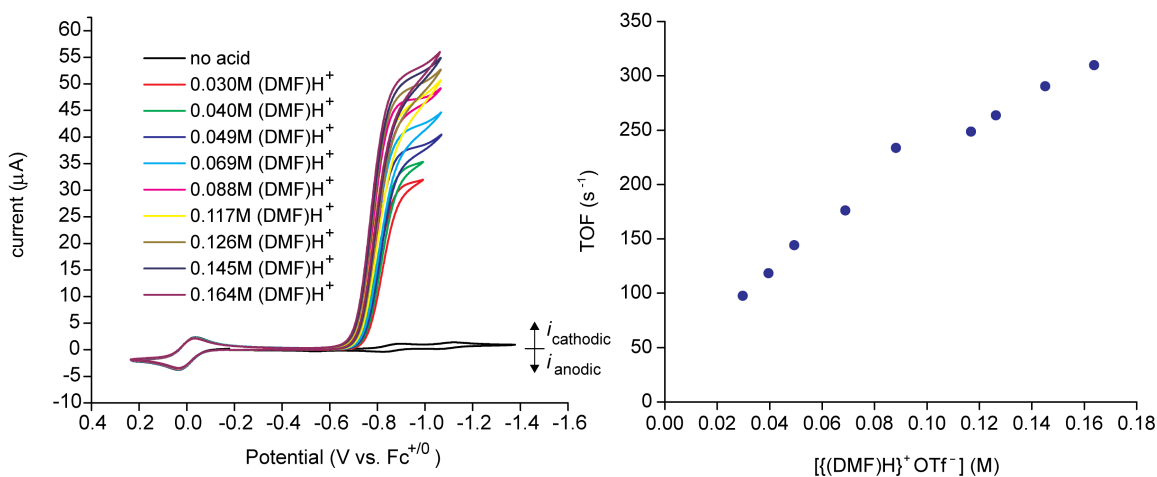


Fig S12

Left: cyclic voltammograms of **1** in CH₃CN (0.1 M ⁿBu₄N⁺PF₆⁻) with 1M H₂O in the presence of varying concentrations of [(DMF)H]⁺OTf⁻ using ferrocene as the internal reference. Scan rate = 0.05 V s⁻¹. Right: plot of the turnover frequency vs. [(DMF)H]⁺OTf⁻.

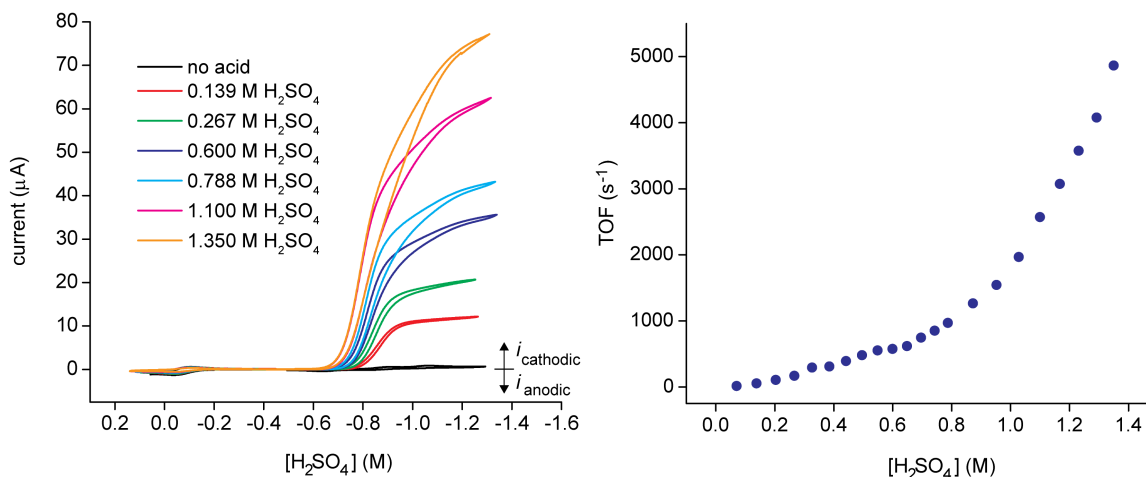


Fig. S13

Left: cyclic voltammograms of **1** in the presence of varying concentrations of H₂SO₄. The solution with no acid (black trace) contains 0.5 mM **1** in H₂O, 50% CH₃CN by volume (0.1 M Na₂SO₄); initial volume = 2.0 mL. Aliquots of 3.6 M H₂SO₄ were added to achieve the desired concentrations. At 1.35 M H₂SO₄ (orange trace) the solution contained 31% CH₃CN by volume. Scan rate for all CVs = 0.05 V s⁻¹. Right: plot of the turnover frequency vs. [H₂SO₄], measured in molarity.

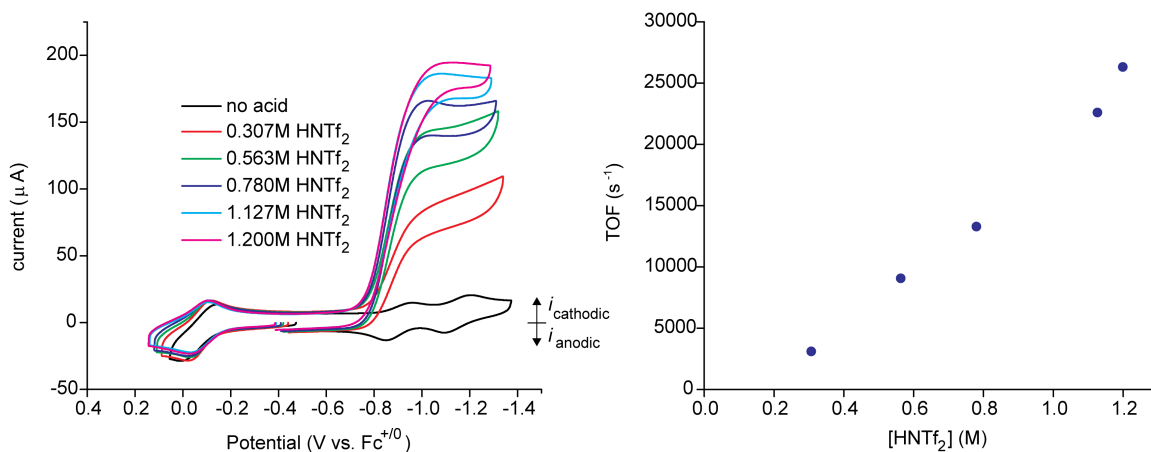


Fig. S14

Left: cyclic voltammograms of **1** in the presence of varying concentrations of HNTf₂. The solution with no acid (black trace) is 0.5 mM **1** in H₂O, 50% CH₃CN by volume (0.1 M LiNTf₂); initial volume = 1.0 mL. Aliquots of 3.4 M HNTf_{2(aq)} were added to achieve the desired concentrations. At 1.200 M HNTf₂ (magenta trace), the solution contained 32% CH₃CN by volume. Scan rate for all CVs= 10 V s⁻¹. Right: plot of the turnover frequency vs. [HNTf₂].

Table S4

Voltammetry data in solvents containing a varying percentage of water. The data demonstrate that i_{cat} is independent of solvent composition between 50% and 70% water. The concentration of HClO_4 for all data is 1.83 M.

% water	[catalyst] (mM)	i_{cat} (A)	$i_{\text{cat}}/[\text{catalyst}]$ (A/mM)
50	0.26	3.69E-04	1.42E-03
55	0.28	4.02E-04	1.44E-03
60	0.40	6.31E-04	1.58E-03
65	0.38	5.73E-04	1.51E-03
70	0.38	5.77E-04	1.52E-03

mean =	1.49E-03
std. dev. =	6.44E-05
% rsd =	4.32

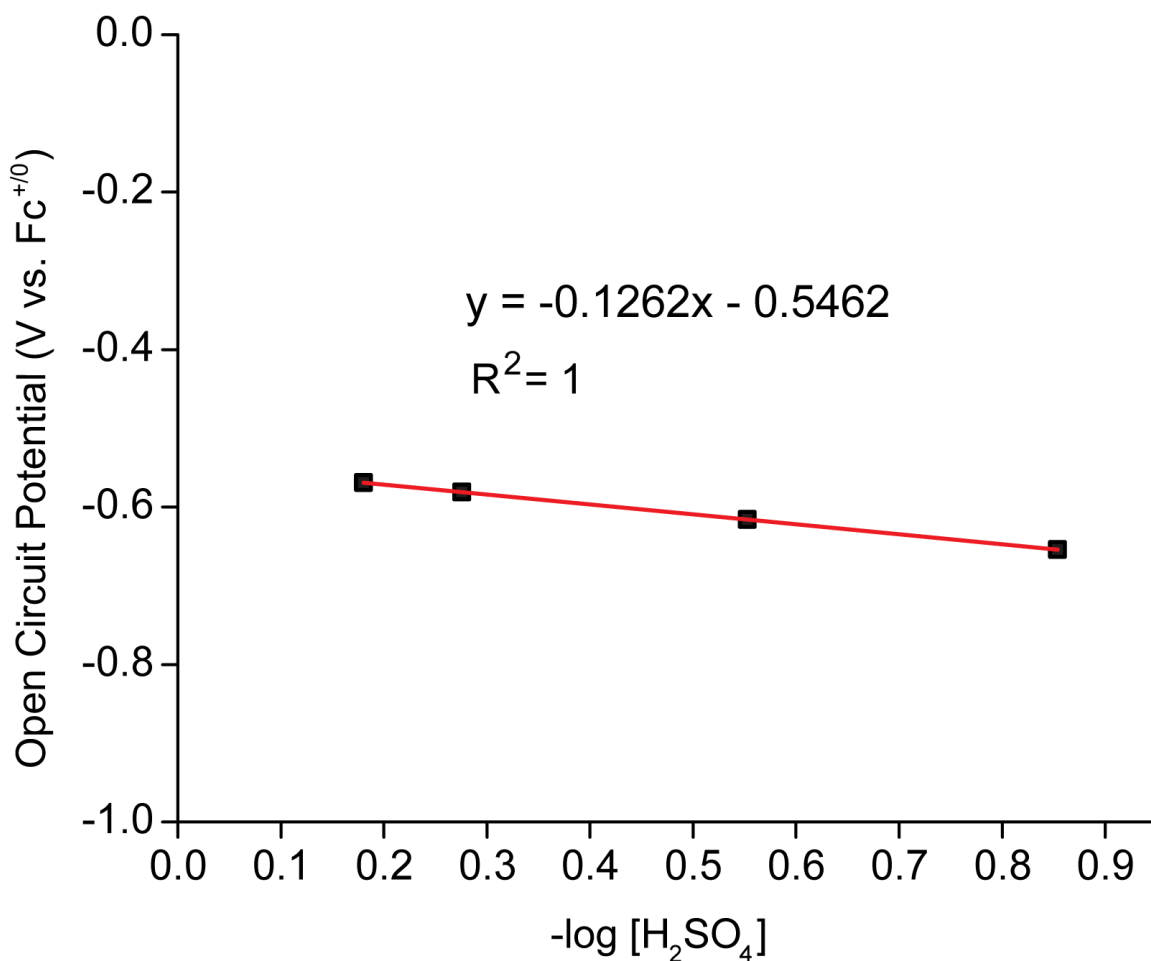


Fig. S15

Plot of the open circuit potential (OCP) at a Pt electrode (E_{H^+/H_2}) vs. $-\log$ of the normality of H₂SO₄. The potentials have been referenced to Fc⁺⁰ by measuring the $E_{1/2}$ of hydroxymethylferrocene ($E_{1/2} = -0.073$ V vs. Fc⁺⁰) immediately following the collection of each OCP data point.

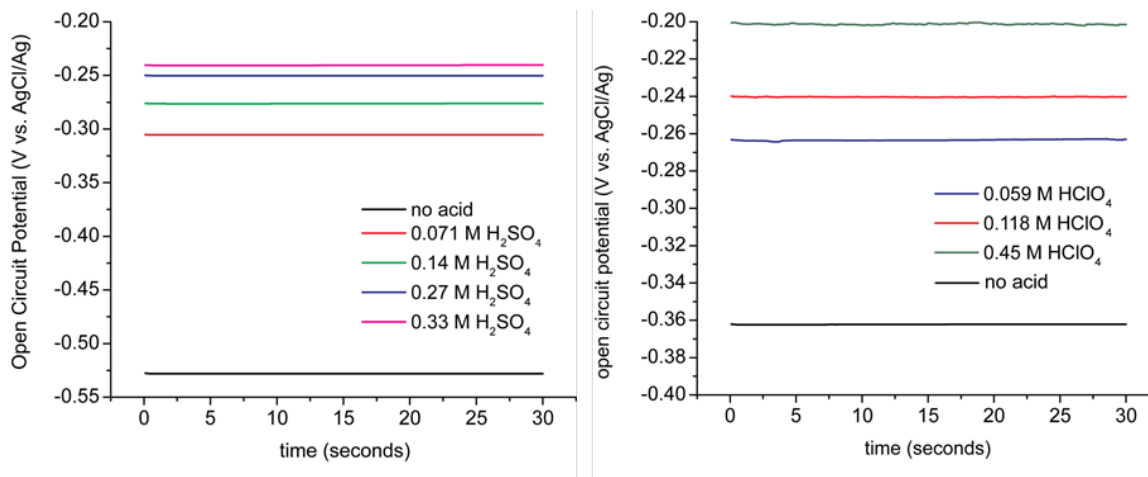


Fig. S16

Open circuit potential (E , vs. AgCl/Ag) at a Pt electrode versus time for solutions initially composed of H₂O, 50% CH₃CN (0.1 M Na₂SO₄) (left) and H₂O, 50% CH₃CN (0.1 M NaClO₄) (right). Aliquots of aqueous sulfuric acid or perchloric acid were added to achieve the desired concentrations. A trace amount of hydroxymethylferrocene was added to each solution as an internal reference. Both solutions were kept under 1 atm H₂ throughout the experiment. Not shown: the OCP in 0.176 M HClO₄ (right) was measured as 0.229 V vs. AgCl/Ag.

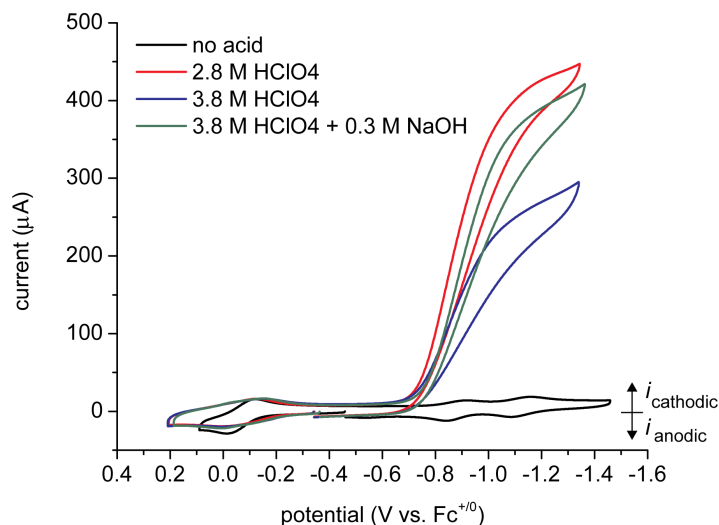


Fig. S17

Cyclic voltammograms of **1** at high concentrations of acid (red and blue traces) and after addition of an aliquot of sodium hydroxide (green trace). The neutralization of excess acid causes the catalytic current to increase, implying that matching the pH of the solution to the pK_a of the pendent amine affords the highest catalytic rates. Scan rate for all CVs is 10 V s^{-1} .

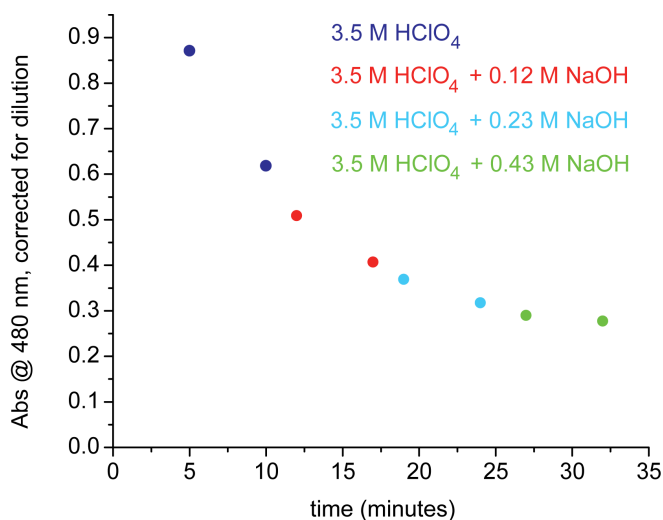


Fig. S18

Plot of the absorbance of at 480 nm for solutions of **1** under highly acidic conditions. As the complex decomposes, aliquots of 4.8 M NaOH are added to the cuvette in order to determine if the decomposition process is reversible. As indicated, the decomposition process is slowed upon successive additions of base, but complex recovery is not observed.

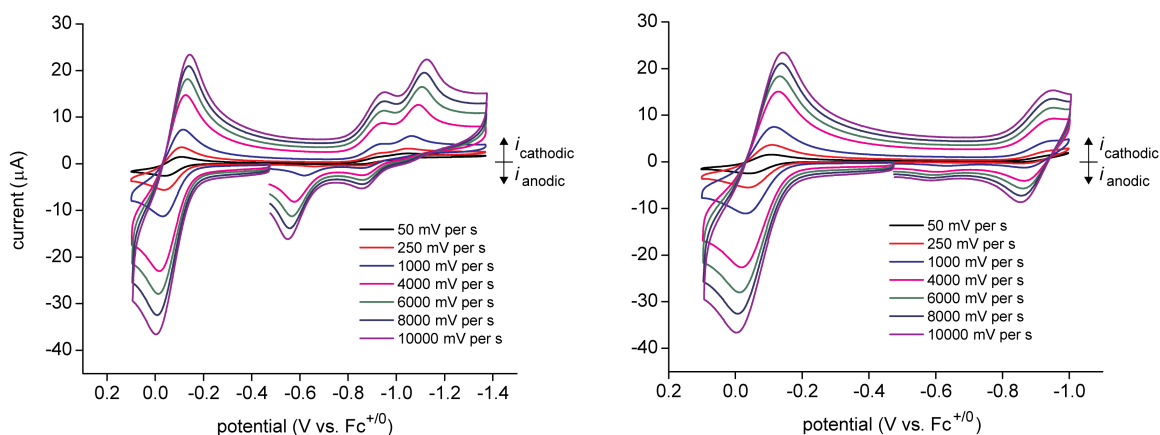


Fig S19.

Left: cyclic voltammograms of **1** and hydroxymethylferrocene in H_2O , 33% CH_3CN by volume (0.1 M NaClO_4) at various scan rates, indicating that the Ni(I/0) redox couple is irreversible. The anodic peak at ca. -0.55 V corresponds to an unidentified species, but the oxidation of a Ni(II) hydride complex is one possibility. Right: cyclic voltammograms of **1** stopping the scan between the two cathodic waves, indicating that the Ni(II/I) couple is chemically reversible and that the new species is formed on reduction of **1** to the Ni(0) oxidation state.

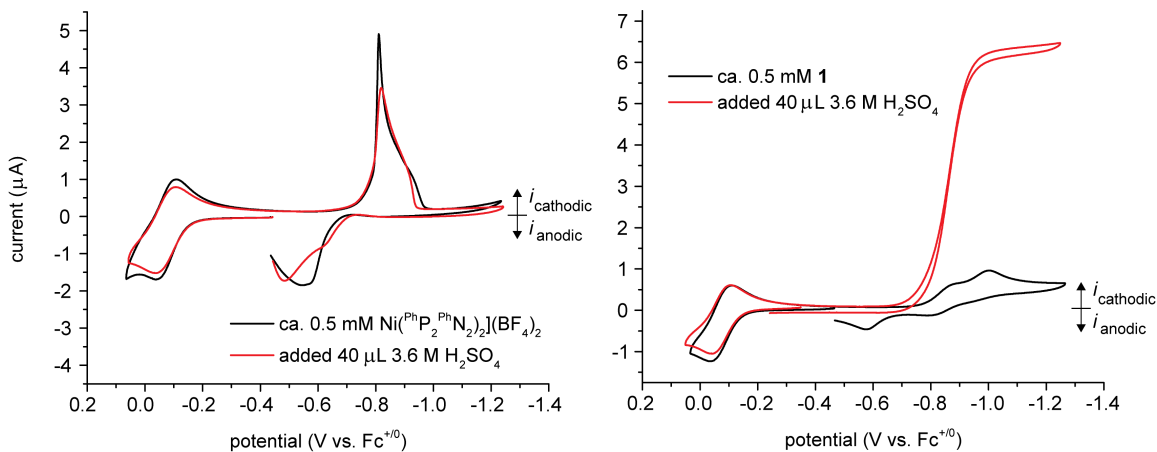


Fig. S20

Left: cyclic voltammograms of ca. 50 mM $[\text{Ni}(\text{P}^{\text{Ph}}_2\text{N}^{\text{Ph}}_2)_2](\text{BF}_4)_2$ in H_2O , 33% CH_3CN by volume (0.1 M Na_2SO_4) (black trace) and with 40 μL 3.6 M H_2SO_4 added (red trace). In both cases, the sharp features in the CVs are consistent with precipitation of the nickel complex. Right: cyclic voltammograms of ca. 0.5 mM **1** in H_2O , 33% CH_3CN by volume (0.1 M Na_2SO_4) and with 40 μL 3.6 M H_2SO_4 added, indicating a soluble, catalytically active complex. Scan rate for all CVs is 0.05 V s^{-1} .

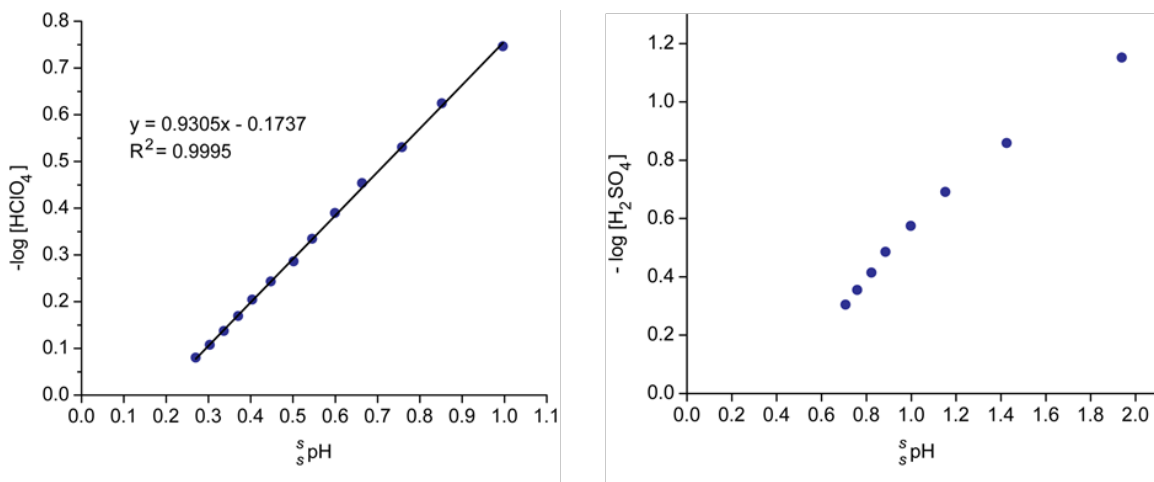


Fig. S21

Correlations between the $-\log [\text{acid}]$ in molarity to the ${}^s\text{pH}$ of the solution for perchloric acid (left) and sulfuric acid (right). At each data point, the pH reading was recorded with a glass pH probe calibrated with aqueous buffer standards at pH 1.0 and 7.0. These readings (${}^w\text{pH}$) were adjusted to ${}^s\text{pH}$ values by the method of Bosch and coworkers.(3)

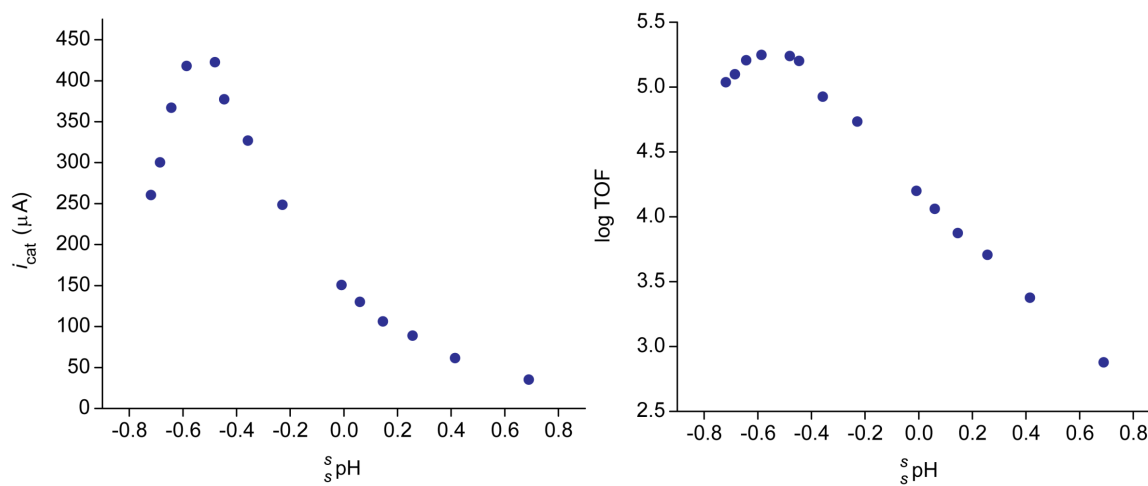


Fig. S22

Plot of the i_{cat} vs. $s_p\text{H}$ (left) and log TOF (measured in s^{-1}) vs. $s_p\text{H}$ (right) for **1**. The $s_p\text{H}$ values were determined by the method of Bosch and coworkers.(3)

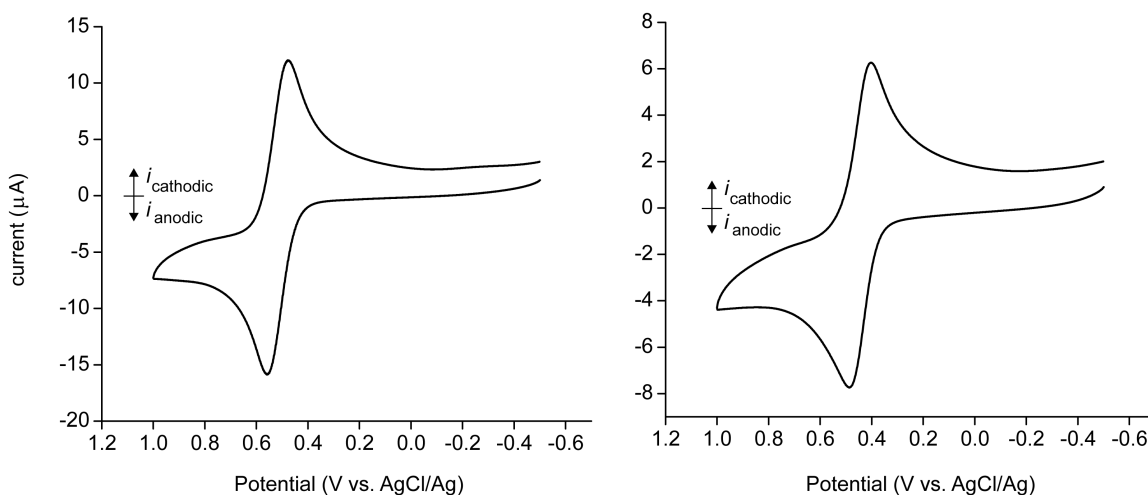


Fig S23.

Since ferrocene is not soluble in the water-acetonitrile electrolyte solutions used here, hydroxymethylferrocene was used as an internal reference compound. Left: CV of ferrocene in CH_3CN ($0.1 \text{ M } n\text{Bu}_4\text{N}^+\text{PF}_6^-$) using a frit-separated reference electrode. The $E_{1/2}$ value is $0.519 \text{ V vs. AgCl/Ag}$. Right: CV of hydroxymethylferrocene taken immediately after the CV of ferrocene under the same conditions as. The $E_{1/2}$ value is $0.446 \text{ V vs. AgCl/Ag}$. Thus, hydroxymethylferrocene $E_{1/2} = -0.073 \text{ V vs. Fc}^{+/0}$. For electrochemical studies presented herein, we assume that the difference in $E_{1/2}$ between ferrocene and hydroxymethylferrocene is medium-independent.

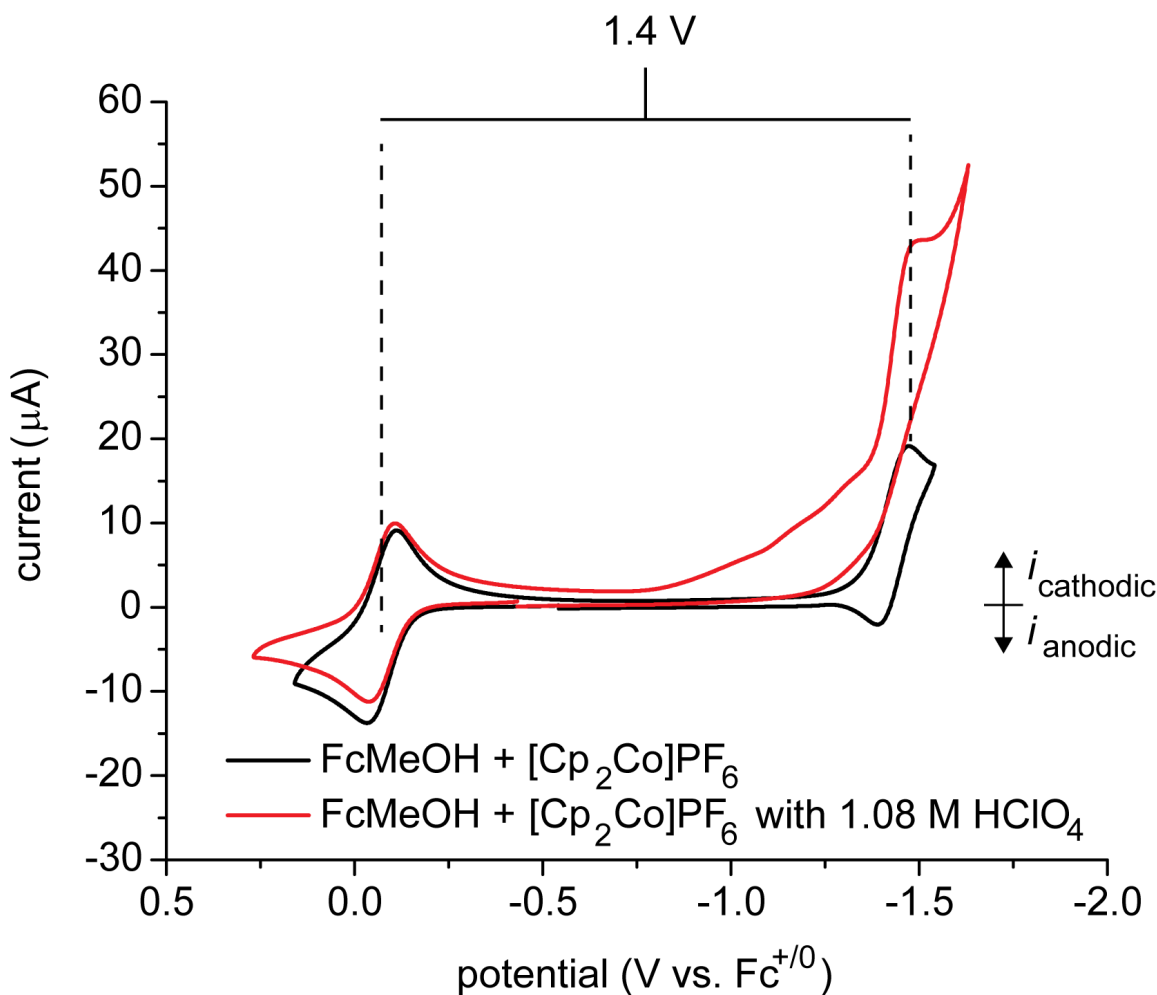


Fig S24.

To test the effect of acid on the $E_{1/2}$ of hydroxymethylferrocene, the electrochemical behavior of solution containing hydroxymethylferrocene and an ostensibly acid-inert redox species (cobaltocenium hexafluorophosphate) was studied in H₂O, 50% CH₃CN by volume (0.1 M NaClO₄). Above, the cyclic voltammograms of solution without acid (black trace) and with acid (red trace) are displayed. Under acidic conditions, the anodic redox peak for the [Cp₂Co]⁺⁰ couple is not observed. However, the potential difference between the cathodic [Cp₂Co]⁺⁰ peak and the $E_{1/2}$ for hydroxymethylferrocene is not significantly different between the two CVs, suggesting that the $E_{1/2}$ for hydroxymethylferrocene stays relatively constant in the presence of acid. Scan rate = 0.1 V s⁻¹.

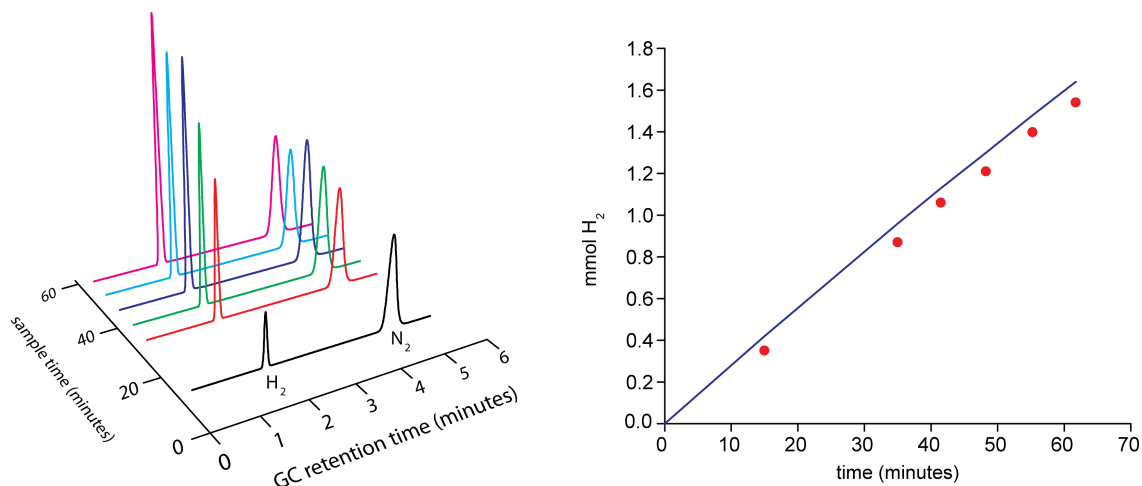


Fig. S25

Left: GC traces for headspace samples of a sealed controlled potential electrolysis cell.
 Right: mmol H₂ observed in each headspace sample (red points) plotted against the mmol H₂ expected for 100% Faradaic efficiency (blue line).

Table S5

Experimental results from a controlled potential electrolysis experiment. Electrolysis was performed at -1.23 V vs. $\text{Fc}^{+/0}$.

Gas sample	1	2	3	4	5	6
Sample time (min)	15.00	35.00	41.50	48.25	55.25	61.75
Charge passed (C)	81.5	185	218	252	286	317
Exp. H ₂ %	2.5	6.2	7.4	8.3	9.5	10.4
Exp. N ₂ %	97.5	93.8	92.6	91.7	90.5	89.6
Exp. Volume H ₂ (mL)	8.1	20.2	24.1	27.0	30.9	33.8
Exp. Volume N ₂ (mL)	316.9	304.8	303.9	298	294.1	291.2
Calc. mmol H ₂	0.42	0.96	1.13	1.30	1.48	1.64
Exp. mmol H ₂	0.35	0.87	1.06	1.21	1.40	1.54
Efficiency (%)	83	91	94	93	95	94
TON (mol H ₂ /mol catalyst)	67	153	180	208	236	262

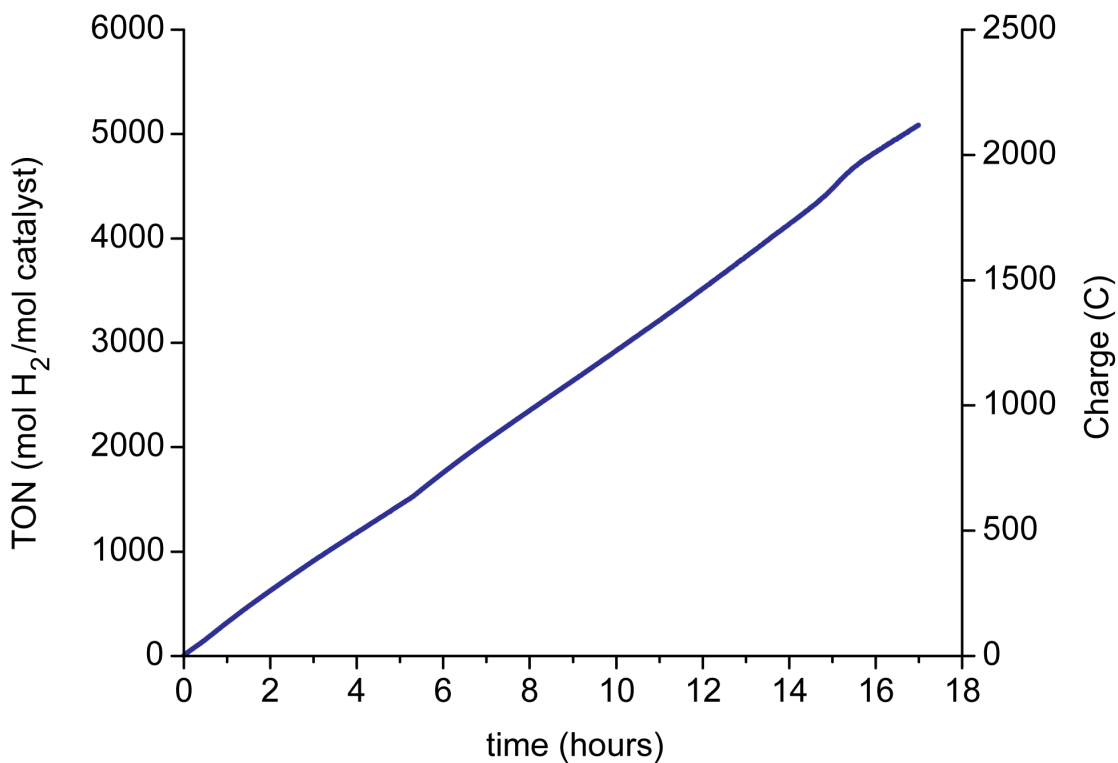


Fig. S26

Electrolysis data for a 43 μM solution of **1** in the presence of 0.66 M HClO_4 at an applied overpotential of 550 mV showing TON vs. time and charge passed vs. time. After 5.3 hours of electrolysis (641 C, 1527 TON), a UV-Vis spectrum of an aliquot of the solution indicated 4% sample decomposition. After 17 hours (2134 C, 5081 TON), the electrolysis was stopped. After 17 hours, colored by-products from Ni-chrome wire (counter electrode) oxidation had diffused into the sample compartment, preventing further UV-Vis analysis.

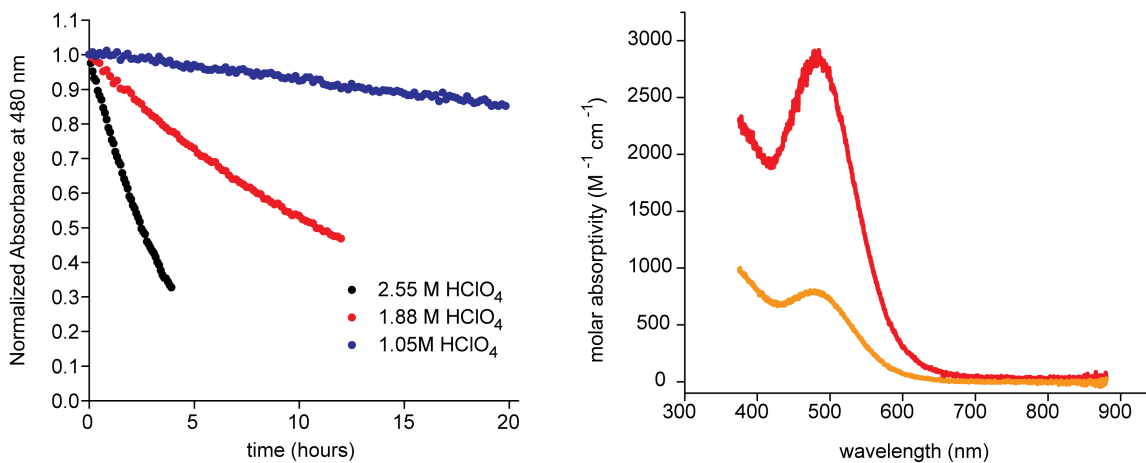


Fig. S27

Left: plots of the normalized absorbance at λ_{\max} (480 nm) versus time in the presence of varying degrees of perchloric acid. Right: visible absorption spectra of **1** in the presence of 2.55 M HClO₄ at t = 0 hr (red trace) and 4 hr (orange trace).

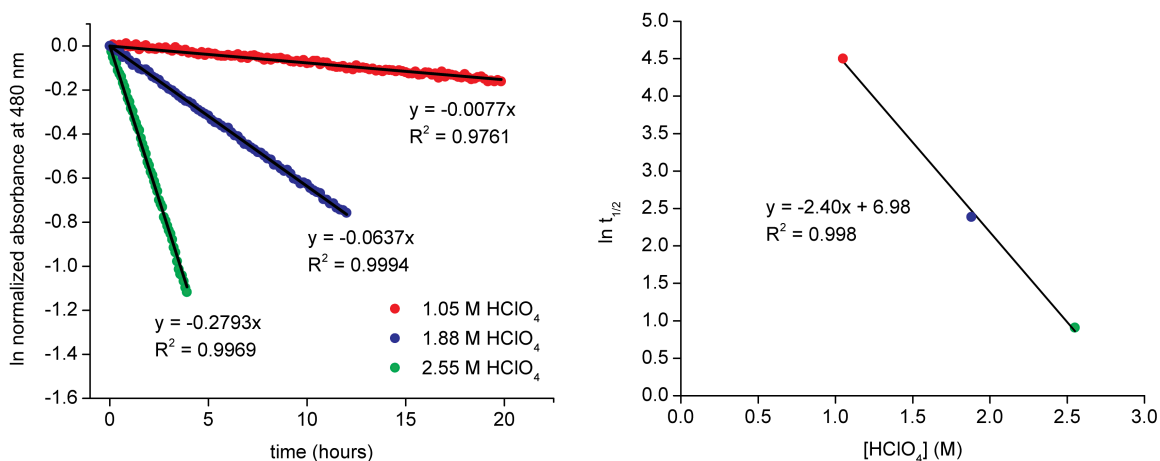


Fig. S28

Left: plots of the natural logarithm of the normalized absorbance values for **1** at λ_{\max} (480 nm) in 1.05M, 1.88M, and 2.55M HClO₄. The y-intercepts for the linear regressions were fixed at 0. From the linear regressions, the half-lives were calculated ($t_{1/2} = \ln 2/|\text{slope}|$) as 2.5 h (2.55M HClO₄), 10.9 h (1.88M HClO₄), and 90.0 h (1.05M HClO₄). Right: plot of $\ln t_{1/2}$ vs. [HClO₄] and the corresponding linear regression.

wh3-33_2ndcrop_31P_THF
STANDARD CARBON PARAMETERS

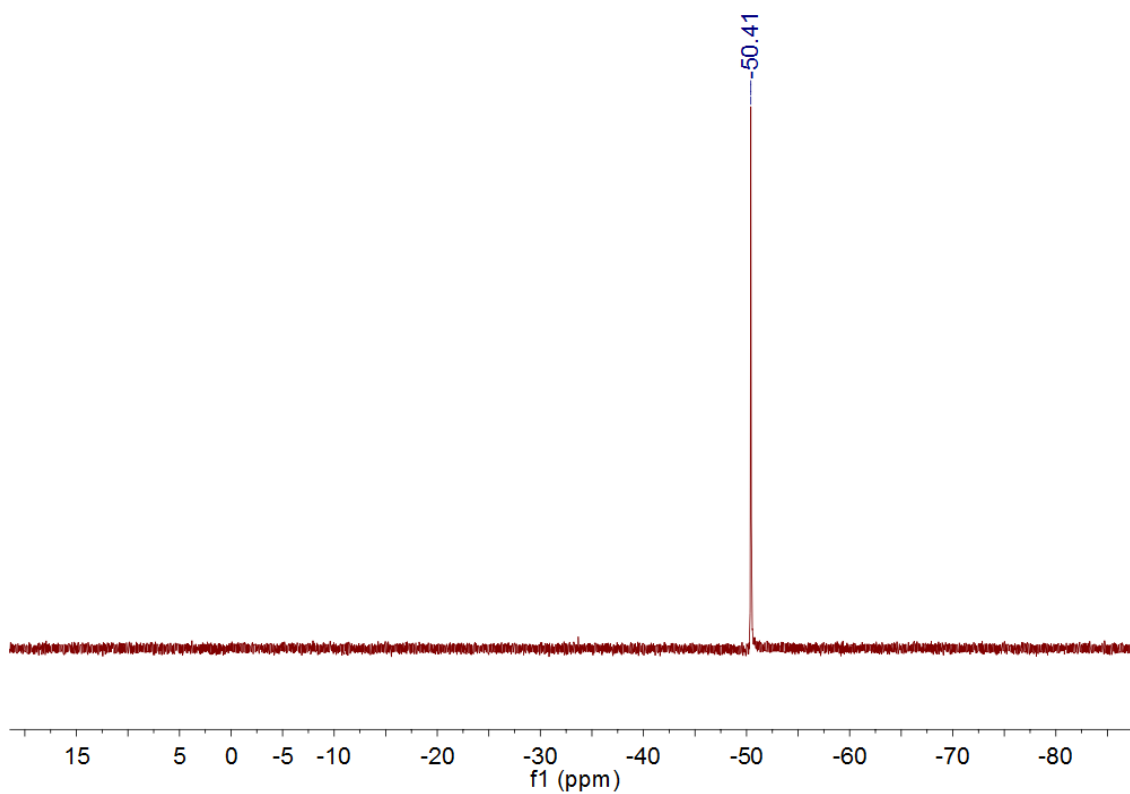


Fig. S29

$^{31}\text{P}\{^1\text{H}\}$ NMR spectrum of $\text{P}^{\text{Ph}}_2\text{N}^{\text{C}_6\text{H}_4\text{OH}}_2$ ligand in THF.

wh3-33_1stcrop_1H_THF
STANDARD CARBON PARAMETERS

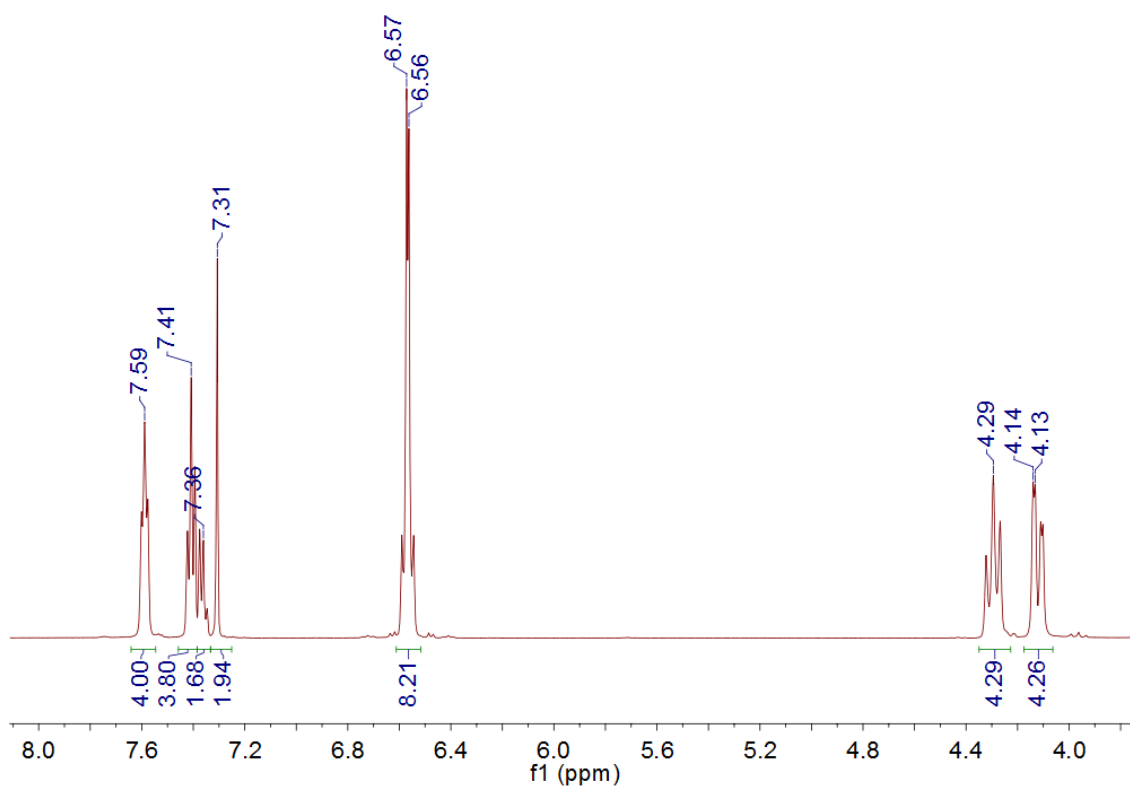


Fig. S30

¹H NMR spectrum of P^{Ph}₂N^{C₆H₄OH}₂ ligand in d₈-THF.

wh3-77_31P_MeCN
STANDARD CARBON PARAMETERS

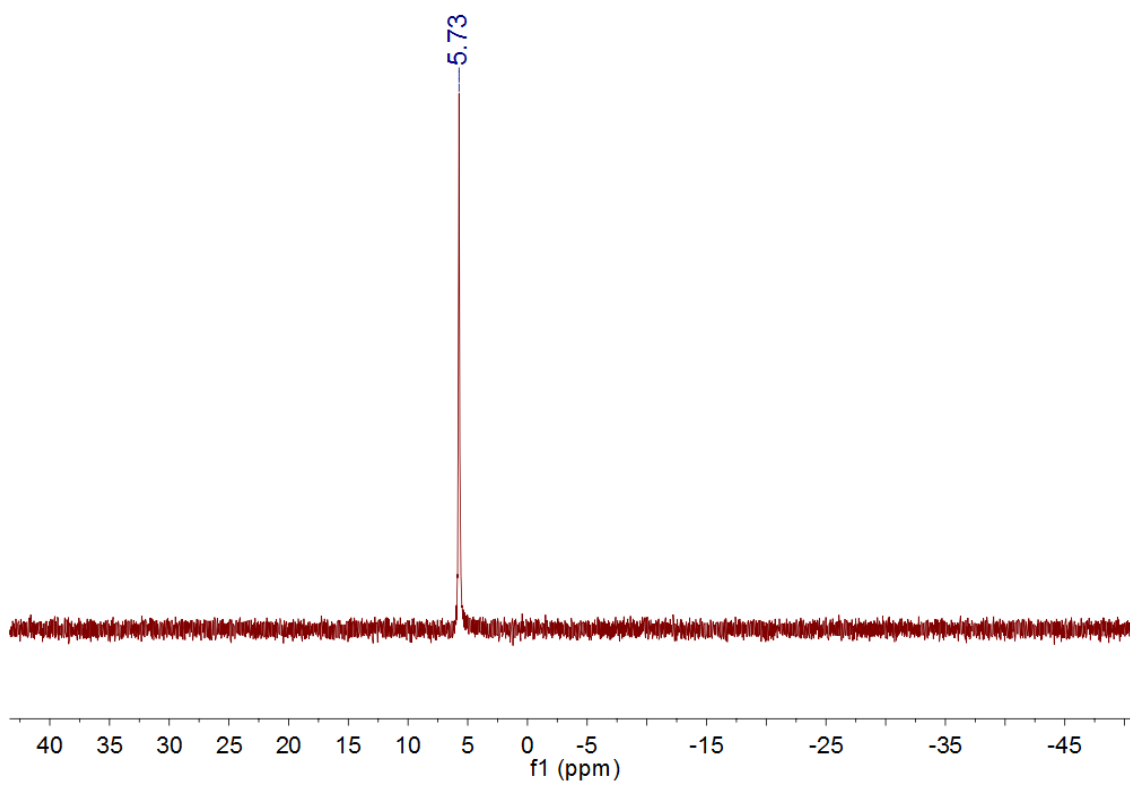


Fig. S31

$^{31}\text{P}\{^1\text{H}\}$ NMR spectrum of complex **1** in CH_3CN .

wh3-77_1H_CD3CN
STANDARD CARBON PARAMETERS

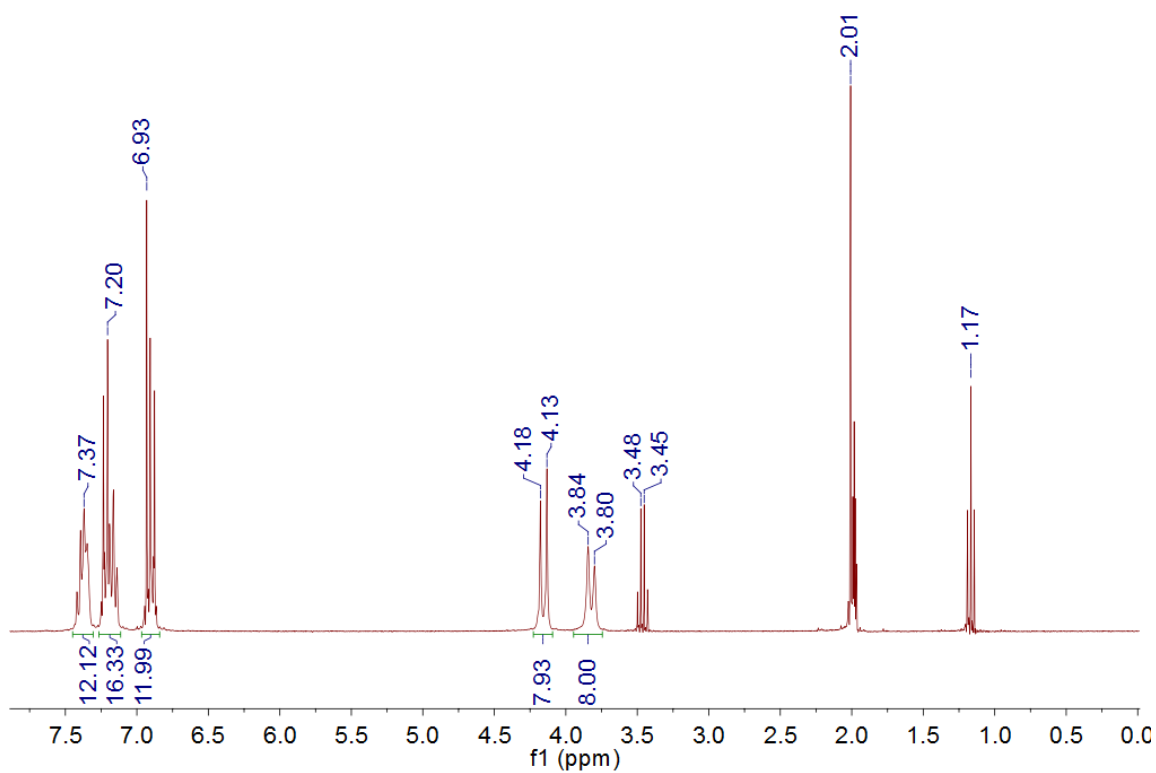


Fig. S32

¹H NMR spectrum of complex **1** in CD₃CN. The resonances at 3.45 and 1.17 ppm correspond to trace diethyl ether. The resonance at 2.01 ppm corresponds to CH₃CN.

Table S6

Crystallographic data^a for complex **1** · (Et₂O)_{1.6}.

Empirical formula	C _{64.4} H ₇₅ B ₂ F ₈ N ₅ NiO _{5.6} P ₄
fw (g/mol)	1364.90
color, habit	red plate
<i>T</i> (K)	130(2)
space group	<i>C</i> 222
<i>Z</i>	4
<i>a</i> (Å)	15.1339(14)
<i>b</i> (Å)	23.3855(14)
<i>c</i> (Å)	20.0338(15)
α (deg)	90
β (deg)	90
γ (deg)	90
<i>V</i> (Å ³)	7090.2(9)
<i>R</i> ₁ , ^b w <i>R</i> ₂ ^c (<i>I</i> >2σ)	0.0494, 0.1354
<i>R</i> ₁ , ^b w <i>R</i> ₂ ^c (all data)	0.0617, 0.1428
GOF	1.076
No. reflections measured	6038
No. of independent reflections	5920
<i>R</i> _{int}	0.0130
CCDC number	927349

^aObtained with graphite-monochromatized Mo Kα radiation (λ=0.71073 Å). ^b $R_1 = \sum ||F_o| - |F_c|| / \sum |F_o|$. ^c $wR_2 = \{ \sum [w(F_o^2 - F_c^2)^2] / \sum [w(F_o^2)^2] \}^{1/2}$.

Table S7

Selected bond distances and angles for **1**.

Bond distances (Å)		Bond Angles (°)	
Ni(1)-P(1)	2.1986(16)	P(1)-Ni(1)-P(2)	82.40(7)
Ni(1)-P(2)	2.210(2)	P(1)-Ni(1)-P(1)#2	177.89(13)
Ni(1)-N(5) ^{CH₃CN}	2.047(9)	P(1)#2-Ni(1)-P(2)	96.86(7)
Ni(1)····N(1) ^{amine}	3.369		
Ni(1)····N(2) ^{amine}	3.760		

References

1. B. J. Hathaway, D. G. Holah, A. E. Underhill, 468. The preparation and properties of some bivalent transition-metal tetrafluoroborate-methyl cyanide complexes, *J. Chem. Soc.*, 2444–2448 (1962).
2. D. H. Pool, D. L. DuBois, [Ni(P^{Ph}₂N^{Ar}₂)₂(NCMe)][BF₄]₂ as an Electrocatalyst for H₂ Production: P^{Ph}₂N^{Ar}₂ = 1,5-(di(4-(thiophene-3-yl)phenyl)-3,7-diphenyl-1,5-diaza-3,7-diphosphacyclooctane), *J. Organomet. Chem.* **694**, 2858–2865 (2009).
3. S. Espinosa, E. Bosch, M. Rosés, Retention of Ionizable Compounds on HPLC. 5. pH Scales and the Retention of Acids and Bases with Acetonitrile–Water Mobile Phases, *Anal. Chem.* **72**, 5193–5200 (2000).
4. A. L. Spek, Single-crystal structure validation with the program PLATON, *J Appl Crystallogr.* **36**, 7–13 (2003).
5. A. D. Wilson *et al.*, Hydrogen Oxidation and Production Using Nickel-Based Molecular Catalysts with Positioned Proton Relays, *J. Am. Chem. Soc.* **128**, 358–366 (2006).
6. R. S. Nicholson, I. Shain, Theory of Stationary Electrode Polarography. Single Scan and Cyclic Methods Applied to Reversible, Irreversible, and Kinetic Systems, *Anal. Chem.* **36**, 706–723 (1964).